NASA/TM—2002-211686

Optimal Micro-Scale Secondary Flow Control for the Management of High Cycle Fatigue and Distortion in Compact Inlet Diffusers

Bernhard H. Anderson
Glenn Research Center, Cleveland, Ohio

Dennis J. Keller
RealWorld Quality Systems, Cleveland, Ohio

National Aeronautics and
Space Administration

Glenn Research Center

July 2002

The Aerospace Propulsion and Power Program at
NASA Glenn Research Center sponsored this work.

Available from

NASA Center for Aerospace Information
7121 Standard Drive
Hanover, MD 21076

National Technical Information Service
5285 Port Royal Road
Springfield, VA 22100

Available electronically at http://gltrs.grc.nasa.gov/GLTRS

OPTIMAL MICRO-SCALE SECONDARY FLOW CONTROL FOR THE MANAGEMENT OF HIGH CYCLE FATIGUE AND DISTORTION IN COMPACT INLET DIFFUSERS

Berhard H. Anderson
National Aeronautics and Space Administration
Glenn Research Center
Cleveland, Ohio 44135

Dennis J. Keller
RealWorld Quality Systems
Cleveland, Ohio 44116

ABSTRACT

The purpose of this report on micro-scale secondary flow control (MSFC) is to study the aerodynamic behavior of micro-vane effectors through their factor (i.e. the design variable) interactions and to demonstrate how these statistical interactions, when brought together in an optimal manner, determine design robustness. The term micro-scale indicates the vane effectors are small in comparison to the local boundary layer height. Robustness in this situation means that it is possible to design fixed MSFC robust installation (i.e. open loop) which operates well over the range of mission variables and is only marginally different from adaptive (i.e. closed loop) installation design, which would require a control system. The inherent robustness of MSFC micro-vane effector installation designs comes about because of their natural aerodynamic characteristics and the manner in which these characteristics are brought together in an optimal manner through a structured *Response Surface Methodology* design process. In the 1950s and 1960s, a collection of analytical and statistical experimental design tools were developed for which the term *Response Surface Methodology* (RSM) was coined. RSM provides an economical, reliable and systematic approach to variable screening as well as the general exploration of the region that contains the estimated optimal conditions. One critical aspect of RSM is its ability to study statistical interactions among the factors (design variables). These statistical interactions often indicate a potential for achieving a robust installation design. A statistical interaction exists between two independent factor variables X_1 and X_2 when the effect of X_1 on response Y_i is affected by the value of X_2. In other words, the effect of factor X_1 on response Y_i is not unique, but changes as a function factor X_2. This is often called a synergistic effect, and it is very important in MSFC installation design.

The band interactions in multi-band MSFC installation designs for two different bands spacing configurations ($\Delta X/c = 4.0$ and $\Delta X/c = 2.0$) were such that strong factor interactions resulted for the engine face distortion (DC60). These interaction were characterized by the behavior than when the "base" band of micro-vane effectors were set to 2.0 mm, the DC60 engine face distortion was not appreciable affected by increases in the micro-vane effector heights in the adjacent upstream bands. In other words, once the vortices generated by the micro-vane effectors balanced the natural secondary flow in the inlet, (i.e. DC60 $\leq$ 0 10), the engine face distortion was

not altered with further increases in strength of the adjacent upstream installation bands. With this factor interaction, it is possible to increase the "strength" of the installation bands to accommodate a stronger inlet secondary flow field resulting from a different mission condition without altering the performance at the original mission condition. Thus, this interaction for engine face distortion (DC60) indicated a potential for achieving a fixed robust installation design able to accommodate an angle-of-incidence variation without significantly effecting engine face distortion. The potential for achieving a truly robust installation design with a fixed micro-vane effector configuration was realized by using optimal robustness techniques in conjunction with *Response Surface Methodologies.*

To illustrate the potential of *Response Surface Methodology* and robustness techniques for secondary flow installation design and robust optimization, two different mission strategies were considered for the subject inlet, namely (1) Maximum Performance, and (2) Maximum HCF Life Expectancy. The Maximum Performance mission sought to minimize the inlet duct losses (i.e. maximize the engine face total pressure recovery, (PFAVE) subject to the constraint that the engine face distortion DC60 to be equal to or less than 0.10. For this mission no constraints were placed on the first five Fourier harmonic 1/2 amplitudes of distortion. The Maximum HCF Life Expectancy mission sought to minimize the mean of the first five Fourier harmonic amplitudes, (i.e. collectively reduced all the Fourier harmonic 1/2 amplitudes of distortion). This mission was also subject to the constraint that the DC60 engine face distortion to be equal to or less than 0.10. No constraint was placed upon the inlet total pressure recovery (PFAVE) for this mission. For each mission strategy, two installation band spacing configurations were studied, i.e. $\Delta X/c = 4.0$ and $\Delta X/c = 2.0$. The purpose of the two installation band configurations was to determine how close the bands can be positioned before the inlet performance degraded. There was essentially the same inlet performance trade-off between the solution for the Maximum Performance and the Maximum HCF Life Expectancy installation designs at each of the bands spacing configurations (i.e. $\Delta X/c = 4.0$ and $\Delta X/c = 2.0$). While the inlet total pressure recovery (PFAVE) was about 0.21% higher for the Maximum Performance mission, the Fourier harmonic 1/2 amplitudes of engine face distortion were also collectively 4.7% higher. The Maximum HCF Life Expectancy installation design was indeed able to collectively reduce the Fourier harmonic 1/2 amplitudes of engine face distortion, but at a cost of a reduction of total pressure recovery (PFAVE). Each of the four optimal robust mission designs (i.e. optimal Maximum Performance and the Maximum HCF Life Expectancy each at band spacings of $\Delta X/c = 4.0$ and $\Delta X/c = 2.0$) were able to maintain a near constant engine face distortion (DC60) over the angle-of-incidence range. For both the Maximum Performance and the Maximum HCF Life Expectancy optimal robust installation designs, a statistical comparison between the DOE models for the $\Delta X/c = 4.0$ and $\Delta X/c = 2.0$ set of configurations indicated that the performance results were not statistically different. In other words, no performance penalty could be statistically established as a result of compressing the band spacing to within one chord length of each other, i.e. $\Delta X/c = 2.0$.

The ability to develop such robust installation designs is a consequence of the factor interactions described in this report. In order to successfully understand these interactions and put them together to achieve a design advantage requires a structured approach to design. That structured approach to MSFC design is satisfied by *Response Surface Methodologies* and *Robustness Design Concepts.*

INTRODUCTION

The current development strategy for combat air-vehicles is directed towards reduction in the Life-Cycle Cost (LCC) with little or no compromise to air-vehicle performance and survivability. This strategy has been extended to the aircraft component level, in particular, the engine inlet diffuser system. One method to reduce inlet system LCC is to reduce its structural weight and volume. Consequently, advanced combat inlet configurations are being made more compact (or shorter) to achieve weight and volume (and LCC) reduction. However, compact S-duct diffusers are characterized by high distortion and low pressure recovery produced by extreme wall curvature and strong secondary flow gradients. These characteristics are further aggravated by maneuver conditions. Since survivability requirements often drive the inlet design towards exotic, non-aerodynamic shapes, it is expected that the flow quality entering the turbine engine will present an additional challenging environment for both fan/compressor surge margin and aeromechanical vibration. Interest in High Cycle Fatigue (HCF) research by the US aerospace community has been spurred by discrepancies between the expected durability of engine components compared to that actually experienced in the field. Recognizing that inlet distortion is a forcing function for vibration in the fan components, methods for increasing HCF Life Expectancy can been combined with techniques for inlet recovery and engine face distortion management. Therefore, to enable acceptable performance levels in such advanced, compact inlet diffuser configurations, micro-scale secondary flow control (MSFC) methods are being developed to manage the recovery, distortion, and HCF aspects of these complex flow fields.[1]-[2]

One of the most difficult tasks in the design of MSFC installations for optimal inlet operation is arriving at the geometric placement, arrangement, number, size and orientation of the effector devices within the inlet duct to achieve optimal performance.These effector devices can be either mechanical or fluidic.This task is complicated not only by the large number of possible design variables available to the aerodynamicist, but also by the number of decisions parameters that are brought into the design process. By including the HCF effects into the inlet design process, the aerodynamicist has a total of seven individual response variables which measure various aspect of inlet performance. They include the inlet total pressure recovery, the total pressure recovery distortion at the engine face and the first five Fourier harmonic 1/2 amplitudes of engine face distortion. Each of these responses needs to be either maximized, minimized, constrained or unconstrained while searching for the optimal combination of primary design variable values that satisfy the mission requirements. The design task is further complicated by the existence of hard-to-control factors which effect inlet performance, i.e. the mission variables. The design of inlet systems is usually accomplished at the cruise condition (the on-design condition) while variations from the cruise condition are considered as an off-design penalty. The mission variables that cause the off-design penalty are, for example, inlet throat Mach number (engine corrected weight flow), angle-of-incidence and angle-of-yaw. Numerical optimization procedures that have been successful with some aerodynamic problems give little assistance to the design of micro-scale secondary flow installations. It is very difficult to incorporate large numbers of independent design and response variables into such procedures. Further, they are very expensive to use if the individual CFD experiments are solutions to the full Navier-Stokes equations in three dimensions. However, there is a statistical approach to the problem which combines an optimally sequenced pattern of Design-of-Experiments (DOE), statistical model building, and system optimization called *Response Surface Methodology* (RSM).

In the 1950s and 1960s, Box[3]-[4] and co-workers developed a collection of analytical and statistical experimental design tools for which the term *Response Surface Methodology* (RSM) was coined. RSM provides an economical, reliable and systematic approach to variable screening as well as the general exploration of the region that contains the estimated optimal conditions. As a result, the pragmatic use of RSM places a high priority on obtaining a better understanding of the process system as well as estimating the optimum conditions. A critical aspect of RSM is its ability to study statistical interactions among the design factors. These interactions often indicate a potential for achieving a robust installation design. A statistical interaction exists between two independent factor variables X_1 and X_2 when the effect of X_1 on response Y_i is affected by the value of X_2. In other words, the effect of factor X_1 on response Y_i is not unique, but changes as a function factor X_2. This is often called a synergistic effect, and it is very important in MSFC installation design.

In this research study on MSFC for compact inlet diffusers, three objectives were considered important, namely: (1) to determine the design characteristics of multi-installation micro-scale secondary flow control configurations, (2) to establish the ability of MSFC to manage the aeromechanical effects of engine face distortion, and (3) to evaluate the effectiveness of robust methodologies to design fixed "open loop" MSFC installation designs in comparison to adaptive "closed loop" designs which would require a control system. This report covers the first two research objectives while Anderson and Keller[5]-[6] covers the third objective and describes a robust design methodology whereby the hard-to-control mission variables can be explicitly included in the design of optimal MSFC installations. A forth report in this series by Anderson and Keller[7] evaluates the impact of engine face rake geometry (i.e. number of rake arms) and its use (i.e. with and without clocking), on the random and systematic measurement errors associated with estimating the first five Fourier harmonic 1/2 amplitudes of engine face distortion. It was concluded in Anderson and Keller[5]-[6] that micro-scale secondary flow control using multi-bands of micro-vane effectors were inherently robust, provided the installations was optimally designed. robustness in this situation means that it is possible to design fixed MSFC robust installations (i.e. open loop) which operates well over the range of mission variables and is only marginally different from adaptive (i.e. closed loop) installation designs which would require a control system. The inherent robustness of MSFC micro-vane effector installation designs comes about because of their natural aerodynamic characteristics and the manner these characteristics are brought together in an optimal manner through a structured *Response Surface Methodology* design process. It is the purpose of this report, therefore, to document the aerodynamic behavior of micro-vane effectors through their factor (i.e. the design variable) statistical interactions and demonstrate how these interactions, when brought together in an optimal manner, determine design robustness.

To illustrate the potential of *Response Surface Methodology* (RSM) and *Robustness Design Concepts* (RDC) to design and optimize robust MSFC installations, two different mission strategies were considered for the subject inlet, namely (1) Maximum Performance, and (2) Maximum HCF Life Expectancy. The Maximum Performance mission sought to minimize the inlet duct losses (maximize the engine face total pressure recovery) subject to the constraint that the DC60 engine face distortion equal to or less than 0.10. This Maximum Performance mission placed no conditions on the first five Fourier harmonic 1/2 amplitudes of distortion. A DC60 distortion level of 0.10 is significant because it would be acceptable for a commercial engine application. The Maximum HCF Life Expectancy mission sought to minimize the mean of the first five Fourier harmonic 1/2 amplitudes, (i.e. collectively reduce all the Fourier harmonic 1/2 amplitudes of distortion).This mission was also subject to the constraint that the DC60 engine face

distortion to be equal to or less than 0.10, but no constraint was placed upon the inlet total pressure recovery.

NOMENCLATURE

AIP	Aerodynamic Interface Plane
c	Micro-Vane Effector Chord Length
CCF	Central Composite Face-Centered
CFD	Computational Fluid Dynamics
D	Engine Face Diameter
DC60	Circumferential Distortion Descriptor
DOE	Design of Experiments
h	Micro-Vane Effector Blade Height
HCF	High Cycle Fatigue
Fi/2	Fourier Harmonic 1/2 Amplitude
FM/2	Mean Fourier Harmonic 1/2 Amplitude
L	Inlet Diffuser Length
LCC	Life Cycle Costs
MSFC	Micro-Scale Secondary Flow Control
Mt	Inlet Throat Mach Number
n	Number of Micro-Vane Effectors per Band
PFAVE	Inlet Total Pressure Recovery
R	Inlet Throat Radius
Re	Reynold Number per ft.
RSM	Response Surface Methodology
α	Inlet Angle-of-Incidence
β	Micro-Vane Effector Angle-of-Incidence
γ	Inlet Angle-of-Yaw

RESULTS AND DISCUSSION

Design of the Experiment

The basic inlet flowpath chosen for this study featured a compact (L/D =3.0), two turn, or S-duct inlet diffuser, Figure (1). This S-duct was defined by AGARD FDP Working Group 13 Test Case 3, Willmer, Brown and Goldsmith[8], and was dubbed the DERA/M2129 inlet. Traditionally, this type of compact inlet duct would be excluded from design consideration since it is characterized by severe wall curvature that induces strong secondary flows. These strong secondary flow can cause a flow separation called vortex lift-off. See Figure (1). This type of 3D flow separation results in total pressure losses and severe engine face distortion. It is not necessary for this vortex to "lift-off" or separate from the walls for high total pressure loss and distortion to occur (hence the terminology inlet "secondary flow control" rather than "separation control". Figure (2) presents the engine face total pressure recovery contours and secondary flow velocity vectors for the DERA/M2129 inlet S-duct at a throat Mach number of 0.70 and at 0^{o}

angle-of-incidence. A vortex pair was dominant in the engine face flow field which was accompanied by very severe engine face total pressure distortion.

To manage the flow in the DERA/M2129 inlet S-duct, two different micro-vane installation configurations were considered. See Figures (3) through (6). For each configuration, a three-band arrangement of micro-vane effectors was placed in the upstream section near the inlet throat. See Figures (3) and (5). For the first configuration, the spacing between the bands of micro-vane effectors were $\Delta X/c = 4.0$, i.e. about four effector chord lengths as measured between the half chord stations. See Figure (4). In the second configuration, the spacing between the bands of micro-vane effectors was $\Delta X/c = 2.0$, i.e. about two micro-vane chord lengths as measured between the half chord stations. See Figure (6). The purpose of the two installation band configurations (i.e. $\Delta X/c = 4.0$ and $\Delta X/c = 2.0$) was to determine how close the bands can be positioned before the inlet performance degraded. These micro-vane effectors were simple micro-vanes, the largest height being about the average height of the momentum layer at the band (3) location, or 2.0 mm with a chord length of 16.0 mm. The purpose of these simple micro-vanes was to create a set of co-rotating vortices that would quickly merge to form a thin layer of secondary flow that would counter the formation of the passage vortex. Since the height of the micro-vane effectors were limited to 2.0 mm, a multi-band arrangement was chosen to investigate the possibility of enhancing the effect of the individual micro-vanes by adding more bands of effectors. The location and spacing between the bands was critical since interaction between respective bands of effector units were anticipated. In the first installation, the first band was placed at the inlet throat station, $X/R = 0.0$, while the second and third bands of effector micro-vanes were placed nominally at $X/R = 1.0$ and at $X/R = 2.0$ respectively. See Figure (3). In the second installation geometry, the first band was placed at the inlet throat station, $X/R = 1.0$, while the second and third bands of micro-vane effectors were placed nominally at axial locations $X/R = 1.5$ and at $X/R = 2.0$ respectively. See Figure (5). Notice that the distance between the respective bands of micro-vane-effectors was compressed in the second installation by keeping the location of the third band fixed in the nominal position $X/R = 2.0$, and shifting the second band downstream one half inlet throat radius, i.e. $\Delta X/R = 0.5$, while shifting the first band downstream one inlet throat radius, i.e. $\Delta X/R = 1.0$. In this study, the "base" band was considered to be band number (3), since its location within the inlet did not change between the $\Delta X/c = 4.0$ and $\Delta X/c = 2.0$ installation configurations.

The DOE approach followed directly from the three objectives previously stated and was reflected in the layout of the design factors listed in Table (1). The design variables (factors) were the micro-vane effector heights (mm) in the three upstream installation h_1, h_2, and h_3, the inlet angle-of-incidence α, and the inlet Reynolds number per ft. (Re). The micro-vane effector heights were changed independently and, therefore, constituted three independent variables. Strictly speaking, the inlet angle-of-incidence, and the Reynolds number were mission variables and were, therefore, the noise factors that belonged with the environmental variables, i.e. the outer array in the traditional Taguchi-style DOE design. Table (2) shows the variables that were held constant during this study. The number of micro-vane effectors, $n_{i,\ i=1,3}$, was held fixed at 24 in the half-plane, and were spaced symmetrically around the half-plane periphery. Each micro-vane effector was set at a geometric micro-vane angle-of-incidence $\beta_{i,\ i=1,3}$ of 24.0°. In addition, the throat Mach Number (Mt), and the inlet angle-of-yaw (γ) were set constant at 0.700, and 0.0° respectively for this investigation. Table (3) displays the response variables for this study. They were the inlet total pressure recovery (PFAVE), the engine face distortion (DC60), and the first five Fourier harmonic 1/2 amplitudes (F1/2, F2/2, F3/2, F4/2, and F5/2) of engine face distortion.

The DOE chosen for each installation was a Central Composite Face-Centered (CCF) in five factor variables. The two DOE's are shown in Tables (4) and (5). They are identical. However, the first and second bands of micro-vane effectors are located at different positions in the inlet S-duct. Notice that these DOE cases covered a substantial range of possible flow situations over a wide range of Reynolds number per ft. (i.e. 4.0×10^6 to 20.0×10^6) and angle-of-incidences (i.e. 0.0^o to 20.0^o). These particular DOE's, like most DOE strategies, varied more than one factor at a time. Further, this layout of 27 cases permitted the estimation of both linear and curvilinear effects as well as interactive or synergistic effects among the DOE factors. This is very important in the study of secondary flow control since very strong interaction effects can develop between separate bands of micro-vane effectors. This CCF DOE strategy is superior to the traditional approach where only changing one variable at a time does not permit the estimation of factor interactions. It is also more economical at 27 runs than a full factorial approach where the number of experiments would be 3^5 or 243 separate CFD cases. Likewise. this DOE is also more economical than a comparable Taguchi approach requiring $6 \times 15 = 90$ runs.

A graphical representation of the Central Composite Face-Centered DOE used in the study is presented in Figure (7). The DOE cases in this figure are represented by the circular symbols, where the symbol locations on the cube signify their factor values. This DOE is called a composite DOE because the organization of cases is composed of a factorial part and a quadratic part. The factorial part of the DOE is composed of 2^5 possible cases, which are represented by the eight corner locations in each of the four corner cubes in Figure (7). Because only half the number of possible factorial cases are actually used in this DOE (circular symbols), the layout is called a fractional factorial and is composed of 2^{5-1} cases. The remaining cases in Figure (7) are the quadratic part. The quadratic cases allow for the evaluation of the curvilinear effects. All together, there are a total of 27 cases in a Central Composite Face-Centered DOE with five factor variables. Notice the balanced layout of cases in Figure (7). This layout of cases represents the smallest number of DOE cases that allows for the evaluation of linear and curvilinear effects as well as interactive or synergistic effects.

Each of the 27 cases in Table (4) and 27 cases in Table (5) were run with a Reynolds-averaged Navier-Stokes code[9] that allowed for numerical simulation of micro-vane effectors without the need to physically embed the micro-vane effectors within the CFD grid structure. For the present study, however, the individual micro-vanes were incorporated into the grid structure, and the appropriate boundary conditions applied to the individual effector micro-vanes.The half-plane grid structure was composed of three blocks: an upstream block, a effector section containing the micro-vanes, and a downstream block. See Figures (3) and (5). The computational half-plane grid varied in total number of mesh points from about 750,000 to 1,500,000 depending on the micro-vane configuration. All CFD calculations were accomplished assuming half-plane symmetry. It was important to investigate the interactions between the separate effector bands without using the micro-vane model in the code, so that proper band interaction could be established. This also established a set of baseline validation data to further verify the micro-vane effector model in the Navier-Stokes code[9] for multi-band flow control design concepts.

To introduce an angle-of-incidence (α-disturbance) into the flow analysis, the condition was imposed that the initial station have an angle-of-incidence component that approximated the measured angle-of-incidence flow field[10]. Even though introducing an α-disturbance into the flow field is not rigorous, it provides a remarkably good approximation in comparison to

the experimental flow field. The overall intent of introducing an α-disturbance into the flow field in this manner was to economically determine the degree of tolerance of the MSFC installation design to angle-of-incidence.

Harmonic Analysis of Distortion

The overall methodology used to obtain the harmonic content of inlet distortion was first proposed by Ludwig[11] and is currently in use at the Williams International Corporation. This methodology is characterized by the use of radial weighting factors applied to the total pressure rake measurements. See Table (6). These radial weighting factors compress the rake information to a single radius ring of data samples, where the number of data samples corresponds to the number of arms of the measurement rake. A separate study was initiated by Anderson and Keller[8] to evaluate the impact of rake geometry (specifically the number of rake arms) on the measurement random and biasing error associated with estimating the first five Fourier harmonic 1/2 amplitudes of engine face distortion. As a result of that study, the rake and methodology chosen for this study was the 80-probe clocked rake because it provided the lowest error in estimating the first five Fourier harmonic 1/2 amplitudes of engine face distortion. The engine face rake total pressure data were obtained by interpolating the 80-probe positions shown in Figure (8a) from the CFD solution. The span-weighted average total pressure was calculated for the 80-probe rake by multiplying the interpolated probe total pressure by the span-weighted coefficients shown in Table (6), and adding the results over the five probes of the rakes to form a single radius ring of data samples. From the engine face patterns at each of the 10 clocking angles, a Fourier analysis was performed, and the mean, standard deviation, and weighting factors were determined for the first five Fourier harmonic 1/2 amplitudes.

Since the rake at the engine face was "clocked", a complete set of "repeats" was generated for each experimental run in Tables (4) and (5). From the engine face patterns at each of the 10 clocking angles, a Fourier analysis was performed on the sample set of data and a standard deviation of the "repeats", S_{clock}, was determined for each of the Fourier harmonic 1/2 amplitudes. In order to check the constant variance assumption associated with standard least square regression, a simple F-test for comparing the minimum standard deviation to the maximum standard deviation ($F = S^2_{max}/S^2_{min}$) was conducted for each of the five responses. The results are presented in Table (7). Since each F-test exceeded the 95% confidence critical value of $F(0.975,9,9) = 4.03$, the assumption of constant variation across the design space had to be discarded. This meant that a regression technique known as weighted least squares regression had to be employed for analyzing the $2 \times 10 \times 27 = 540$ data samples in the two DOE's. The weights in these regression analyses were set to $1/S^2_{clock}$.

The data reduction for the inlet total pressure recovery and engine face distortion differ greatly from the harmonic analysis of distortion described. The reason is that there is no generalized methodology to evaluate the Fourier harmonic amplitudes of engine face distortion for more that five probes in the radial direction. Hence, both the inlet total pressure recovery and engine face distortion were calculated directly from the computational grid at the engine face station. See Figure (8b). The DC60 engine face distortion descriptor[12] is defined such that it can be determined from either a computational grid or a standard measurement rake. It is the only recognized distortion descriptor that has this property, and was the reason it was chosen for this study.

The DC60 engine face distortion descriptor is a parameter commonly used throughout Europe and is usually determined from a 72-probe standard AIP rake.

Micro-Vane Effector Band Interactions

Presented in Figures (9) through (11) are the three possible two way statistical factor interactions that can occur between the micro-vane effector bands. These include the (h_2*h_3) band interaction, the (h_1*h_3) band interaction and the (h_1*h_2) band interaction for both the $\Delta X/c$ = 4.0 and $\Delta X/c$ = 2.0 installation configurations. Comparisons are made in each figure for both the inlet total pressure recovery (PFAVE), and engine face distortion (DC60) characteristics. A statistical interaction exists between two independent factor variables X_1 and X_2 when the effect of X_1 on response Y_i is affected by the value of X_2. In other words, the effect of factor X_1 on response Y_i is not unique, but changes as a function factor X_2.

For example, Figures (9a) and (9b) presents the inlet performance metrics PFAVE and DC60 as a function of the second band height (h_2) at three levels of the third band height (h_3). In this study, the "base" band was considered to be band number (3), since its location within the inlet did not change between the $\Delta X/c$ = 4.0 and $\Delta X/c$ = 2.0 installation configurations. In other words, the band installations between the two designs were compressed towards the "base" band. The effect of the second band installation heights (h_2) was such that it decreased the inlet total pressure recovery (PFAVE) as the second band installation heights (h_2) increased, at each of the three levels of third band heights (h_3). See Figure (9a). However, the rate of decrease of PFAVE did not change at the three levels of third band heights (h_3), Therefore, PFAVE as a function of (h_2) formed three parallel lines at the three levels of (h_3). Since the relationship between PFAVE and h_2 differed only by an additive constant between the three levels of (h_3), there was no (h_2*h_3) statistical interaction for the inlet total pressure recovery (PFAVE). The effect of the second band installation height (h_2) on the engine face distortion (DC60) also decreased as the second band installation heights increased. However, the rate of decrease was strongly affected by the level of the micro-vane heights in the "base" band (h_3). See Figure (9b). The greatest rate of reduction in engine face distortion (DC60) occurred when the micro-vane heights (h_3) were set to zero (solid line in Figure (9b)). When the "base" band heights (h_3) were set to 2.0 mm, (dash-dot line in Figure (9b)), the DC60 engine face distortion was not appreciable affected by the micro-vane heights in the second installation band (h_2). Therefore, a very strong statistical (h_2*h_3) interactions existed for the engine face distortion (DC60). When the micro-vane heights in the third band (h_3) were set to 2 mm, vortices of increasing strength were generated from the second band of micro-vanes as (h_2) increased. However, increasing the strength of the micro-vortices in the second band did not appreciably impact engine face distortion. Therefore, there is a fundamental difference between simply generating micro-vortices and managing engine face distortion. The natural aerodynamics characteristics of properly designed installations of micro-vane effectors are such that once the vortices generated by the micro-vanes balanced the natural secondary flow in the inlet, (i.e. DC60 $\leq$ 0 10), no increases in installation strength will change the engine face distortion.

Presented in Figures (9c) and (9d) are the inlet performance metrics (PFAVE) and (DC60) for the $\Delta X/c$ = 2.0 installation configurations. These figures illustrate the (h2*h3) statistical interaction when the band locations were compressed. Again, there was no statistical (h2*h3)

interaction for inlet total pressure recovery (PFAVE). However, the same strong (h2*h3) statistical interaction occurred for the engine face distortion (DC60). When h_3 was set to 2 mm, the DC60 engine face distortion was again insensitive to the settings on the second band installation heights (h_2). Spacing the micro-vane effector bands closer together did not appreciably alter the factor interactions of the micro-vane effectors.

Figures (10a) through (10d) presents the inlet performance metrics (PFAVE) and (DC60) for both the $\Delta X/c = 4.0$ and $\Delta X/c = 2.0$ installation configurations, These figures illustrates the (h_1*h_3) statistical interaction. Essentially the same interaction characteristics occurred for the (h_1*h_3) as with the (h_2*h_3) interactions. No interactions occurred for the inlet total pressure recovery (PFAVE) but strong (h_1*h_3) interactions occurred for the engine face distortion (DC60) for both installations. Thus spacing the micro-vane effector bands further apart did not appreciably alter the factor interactions of the micro-vane effectors.

Figures (11a) through (11d) illustrate the (h1*h2) interaction regarding the inlet total pressure recovery (PFAVE) and engine face distortion (DC60) when the base band is moved forward an amount $\Delta X/R = 1.0$ and $\Delta X/R = 0.5$. Although the (h_1*h_2) interactions look similar to the both the (h_2*h_3) and (h_1*h_3) presented in Figures (9) and (10), they differ in one important respect. The (h_1,h_2) combination band installation was unable to meet the DC60 $\leq$ 0.10 mission requirement. This was true for both the $\Delta X/c = 4.0$ and $\Delta X/c = 2.0$ installation configurations.

The band interactions in a multi-band MSFC installation designs for two different bands spacing configurations ($\Delta X/c = 4.0$ and $\Delta X/c = 2.0$) were such that strong factor interactions resulted for the engine face distortion (DC60). When the "base" band of micro-vane effectors were set to 2.0 mm, the DC60 engine face distortion was not appreciable affected by increases in the micro-vane effector heights in the adjacent upstream bands. In other words, once the vortices generated by the micro-vane effectors balanced the natural secondary flow in the inlet, (i.e. DC60 $\leq$ 0 10), the engine face distortion was not altered with further increases in strength of the adjacent upstream installation bands. With this factor interaction, it is possible to increase the "strength" of the installation bands to accommodate a stronger inlet secondary flow field resulting from a different mission condition without altering the performance at the original mission condition. Thus, this interaction for engine face distortion (DC60) indicated a potential for achieving a fixed robust installation design able to accommodate an angle-of-incidence variation without significantly effecting engine face distortion. The potential for achieving a truly robust installation design, able to achieve excellent performance over an angle-of-incidence range with a fixed micro-vane effector configuration, is only realized by using optimal robustness techniques.[5]-[6]

Optimal Robust Micro-Vane Effector Installation Design

To illustrate the potential of RSM and robustness considerations to design and optimize MSFC installations, two mission strategies were considered for the subject inlet, namely (1) Maximum Performance, and (2) Maximum HCF Life Expectancy. The Maximum Performance mission minimized the inlet duct losses (maximize the engine face total pressure recovery) subject to the constraint that the DC60 engine face distortion be less than 0.10, while no conditions were placed on the first five Fourier harmonic 1/2 amplitudes of distortion. A DC60 distortion level of 0.10 or less is significant because it would be acceptable for a commercial engine application. The

Maximum HCF Life Expectancy mission minimized the mean of the first five Fourier harmonic 1/2 amplitudes of distortion, i.e. "collectively" reduced the first five Fourier harmonic 1/2 amplitude of distortion. This mission was also subject to the constraint that the DC60 engine face distortion be less than 0.10,while no constraint was placed upon the inlet total pressure recovery. A detailed description of the robust methodology used in the present study appears in Anderson and Keller,[5] and is termed the "Lower Order" method, while a lengthy comparison between the "Lower Order", Taguchi and an alternative "High Order" method appears in Anderson and Keller.[6]

Maximum Performance Mission - The "Optimal Robust" MSFC installation, constrained the engine face distortion to DC60 $\leq$ 0.10, while a search was made over the factor variable space to locate that installation geometry that minimized the mean of inlet duct losses over the range of angle-of-incidences, $\alpha = 0^{\circ}, 1.0^{\circ}, \ldots, 20.0^{\circ}$ i.e.

$$Y_{\alpha} = \frac{1}{N_{\alpha}} \sum_{i=1}^{N_{\alpha}} (1.0 - PFAVE) \qquad (1)$$

where N_{α} is the number of α's in the set $\alpha = 0^{\circ}, 1.0^{\circ}, \ldots, 20.0^{\circ}$. For this mission, no constraints were placed on the first five Fourier harmonic 1/2 amplitudes of engine face distortion. This procedure defined one installation that was "Optimal Robust" over the entire range of angle-of-incidence.

The "Optimal Robust" Maximum Performance $\Delta X/c = 4.0$ installations and their corresponding CFD performance are presented in Tables (10) and was determined through a search process to have the following effector vane heights (mm): $h_1 = 0.0$, $h_2 = 0.0$, $h_3 = 1.9$. The inlet CFD validation engine total pressure recoveries contours solution for the "Optimal Robust" Maximum Performance Optimal $\Delta X/c = 4.0$ installation design at the engine face is presented in Figure (12). A comparison between the near wall streamlines for the baseline configuration and $\Delta X/c = 4.0$ installation design are shown in Figures (13) and (14). A comparison of these figures indicates the underlying operational purpose of micro-scale secondary flow control. In the baseline case presented in Figure (13), the flow in a very thin layer adjacent to the walls "over turns" as a result of a loss of momentum within the inlet boundary layer. Eventually, this "over-turning" will cause a vortex to form in the inlet passage. This vortex causes in total pressure loss and severe total pressure distortion at the engine face. It is not necessary for this vortex to "lift-off" or separate from the walls for high total pressure loss and distortion to occur (hence the terminology inlet "secondary flow control" rather than "separation control"). By introducing the micro-effectors into the inlet, the "over-turning" in the inlet boundary was prevented. See Figure (13) and (14). Consequently, the passage vortex did not form or, at worst, was greatly reduced in strength. Therefore, the entire inlet flow field can be managed by controlling the secondary flow in a thin layer adjacent to the inlet walls. In the MSFC concept, micro-scale actuation is used as an approach called "secondary flow control" to alter the S-duct's inherent secondary flow characteristics with the goal of simultaneously improving the critical system level performance metrics of inlet total pressure recovery, engine face distortion, and HCF characteristics.

Presented in Figures (15) through (17) are the engine face total pressure recovery contours and secondary velocity flow fields for the $\Delta X/c = 4.0$ optimal Robust Maximum Performance installation at angle-of-incidences of 0°, 10.0°, and 20.0°. In general, the $\Delta X/c = 4.0$ optimal robust Maximum Performance installation was able to maintain an engine face total pressure

recovery contour signature that was near uniform distributed around the periphery of the engine face over the 20° angle-of-incidence range of the inlet.

The "Optimal Robust" Maximum Performance $\Delta X/c = 2.0$ installations and the corresponding CFD performance are presented in Table (11) and determined through a search process to have the following effector vane heights (mm): $h_1 = 0.0$, $h_2 = 0.1$, $h_3 = 1.5$. The inlet CFD validation engine total pressure recoveries contours solution for the "Optimal Robust" Maximum Performance Optimal $\Delta X/c = 2.0$ installation design at the engine face is presented in Figure (18). A comparison between the near wall streamlines for the baseline configuration and $\Delta X/c = 2.0$ installation design are shown in Figures (19) and (20). Again, notice the effect of the micro-vane effectors in preventing the over-turning of the flow adjacent to the inlet walls and thus suppressing or weakening the passage vortex formation. Presented in Figures (21) through (23) are the engine face total pressure recovery contours and secondary velocity flow fields for the $\Delta X/c = 2.0$ optimal Robust Maximum Performance installation at angle-of-incidences of 0°, 10.0°, and 20.0°. In general, the $\Delta X/c = 2.0$ optimal Robust Maximum Performance installation was able to maintain an engine face total pressure recovery contour signature that was near uniform distributed around the periphery of the engine face over the 20° angle-of-incidence range of the inlet.

Presented in Figures (24a) through (25h) is a comparison summary of the DOE performance differences between the optimal Robust installation designs for the $\Delta X/c = 4.0$ and $\Delta X/c = 2.0$ configurations over the angle-of-incidence range from 0° to 20.0°. The total pressure recovery (PFAVE) for both optimal robust installation designs fell below the baseline flow solution. See Figure (24a). A comparison between the DOE total pressure recovery characteristics for the $\Delta X/c = 4.0$ and $\Delta X/c = 2.0$ configurations indicate that the $\Delta X/c = 4.0$ installation design had a somewhat higher engine face recovery over the angle-of-incidence range from 0° to 20.0°. Whether this difference is statistically meaningful in discussed in depth in the section entitled "Statistical Comparison of Optimal Robust Installation Designs". A comparison between the engine face distortion (DC60) for both optimal robust installation designs indicates essentially no performance differences. See Figure (24b). Also, the both optimal robust installation designs were able to maintain a near constant DC60 distortion level over the over the angle-of-incidence range from 0° to 20.0°. A comparison of the first five DOE predicted Fourier harmonic 1/2 amplitude is presented in Figures (24c) through (24g) for the $\Delta X/c = 4.0$ and $\Delta X/c = 2.0$ configurations over the angle-of-incidence range from 0° to 20.0°. While performance differences exists between the two optimal robust installation designs, it is presently not known whether these difference would make any impact on engine maintainability. Not enough is presently known about High Cycle Fatigue to make that judgement. However, whether these differences are statistically meaningful are discussed in depth in the section entitled "Statistical Comparison of Optimal Robust Installation Designs". Presented in Figure (24h) is a comparison of the mean of the first five Fourier harmonic 1/2 amplitudes of engine face distortion for the $\Delta X/c = 4.0$ and $\Delta X/c = 2.0$ configurations over the angle-of-incidence range from 0° to 20.0°. The results indicate that the optimal robust Maximum Performance installation designs "collectively" reduced the first five Fourier harmonic 1/2 amplitudes of engine face distortion, and that low level can be maintained over the angle-of-incidence range from 0° to 20.0.° The significance of that characteristic is that the robustness properties of micro-vane effector installations also extends to the Fourier harmonic 1/2 amplitudes of engine face distortion.

Maximum HCF Life Expectancy Mission - The "Optimal Robust" Maximum HCF Life Expectancy MSFC installation constrained the engine face distortion to DC60 $\leq$ 0.10 while a search was made over the factor variable space to locate that installation geometry that minimized the mean of the first five Fourier harmonic 1/2 amplitudes present in the engine face distortion over the range of angle-of-incidences $\alpha = 0^o$, 1.0^o,..., 20.0^o, i.e.

$$Y_\alpha = \frac{1}{N_\alpha} \sum_{i=1}^{N_\alpha} \frac{1}{5} \sum_{j=1}^{5} \left(\frac{Fj}{2}\right)_i \qquad (2)$$

where N_α is the number of α's in the set $\alpha = 0^o$, 1.0^o,..., 20.0^o.

The "Optimal Robust" Maximum HCF Life Expectancy $\Delta X/c = 4.0$ installation and their corresponding CFD performance are presented in Table (12) and was determined through a search process to have the following micro-vane effector heights (mm): $h_1 = 0.2$, $h_2 = 1.0$, $h_3 = 2.0$. The inlet CFD validation engine total pressure recoveries contours solution for the "Optimal Robust" Maximum HCF Life Expectancy Optimal $\Delta X/c = 4.0$ installation design at the engine face is presented in Figure (25). A comparison between the near wall streamlines for the baseline configuration and $\Delta X/c = 4.0$ installation design are shown in Figures (26) and (27). Again, the effect of the micro-vane effectors was to prevent the over-turning of the flow adjacent to the inlet walls and thus suppress the formation of the passage vortex. Presented in Figures (28) through (30) are the engine face total pressure recovery contours and secondary velocity flow fields for the $\Delta X/c = 4.0$ optimal Robust Maximum HCF Life Expectancy installation at angle-of-incidences of 0^o, 10.0^o, and 20.0^o. Even at 20^o angle-of-incidence, the optimal robust $\Delta X/c = 4.0$ installation design can maintain a near uniform circumferential distribution of total pressure recovery (PFAVE). See Figure (30).

The "Optimal Robust" Maximum HCF Life Expectancy $\Delta X/c = 2.0$ installations and their corresponding CFD performance are presented in Table (13) and was determined through a search process to have the following micro-vane effector heights (mm): $h_1 = 0.5$, $h_2 = 0.2$, $h_3 = 2.0$. The inlet CFD validation engine total pressure recovery (PFAVE) contours solution for the "Optimal Robust" Maximum HCF Life Expectancy Optimal $\Delta X/c = 2.0$ installation design at the engine face is presented in Figure (31). A comparison between the near wall streamlines for the baseline configuration and $\Delta X/c = 2.0$ installation design are shown in Figures (32) and (33). The micro-effector Maximum HCF Life Expectancy Optimal $\Delta X/c = 2.0$ installation design prevents the over-turning of the flow adjacent to the inlet walls and thus suppressed the formation of the passage vortex. Presented in Figures (34) through (36) are the engine face total pressure recovery contours and secondary velocity flow fields for the $\Delta X/c = 2.0$ optimal Robust Maximum HCF Life Expectancy installation at angle-of-incidences of 0^o, 10.0^o, and 20.0^o. The suppression of the passage vortex formation by the micro-effector installation reflect itself in a circumstantially uniform distribution of inlet total pressure recovery (PFAVE) at angle-of-incidences of 0^o, 10.0^o, and $20.0.^o$

Presented in Figures (37a) through (37h) is a comparison summary of the DOE performance differences between the optimal robust installation designs for the $\Delta X/c = 4.0$ and $\Delta X/c = 2.0$ configurations over the angle-of-incidence range from 0^o to 20.0^o. The total pressure recovery (PFAVE) characteristics for both optimal robust installation designs again fell below the baseline flow solution. See Figure (37a). A comparison between the DOE total pressure recovery

characteristics for the $\Delta X/c = 4.0$ and $\Delta X/c = 2.0$ configurations indicate that the $\Delta X/c = 4.0$ installation design had a somewhat higher engine face recovery over the angle-of-incidence range from 0° to 20.0°. Whether this difference is statistically meaningful in discussed in depth in the section entitled "Statistical Comparison of Optimal Robust Installation Designs".A comparison between the engine face distortion (DC60) for both optimal robust installation designs indicates essentially no performance differences. See Figure (37b). Also, the both optimal robust installation designs were able to maintain a near constant DC60 distortion level over the over the angle-of-incidence range from 0° to 20.0°, which meets the mission requirements $DC690 \leq 0.10$ and which is dramatically lower that the baseline distortion characteristics. A comparison of the first five DOE predicted Fourier harmonic 1/2 amplitude is presented in Figures (37c) through (37g) for the $\Delta X/c = 4.0$ and $\Delta X/c = 2.0$ configurations over the angle-of-incidence range from 0° to 20.0°. While performance differences exists between the two optimal robust installation designs, it is presently not known whether these difference would make any impact on engine maintainability. Not enough is presently known about High Cycle Fatigue to make that judgement. However, whether these differences are statistically meaningful are discussed in depth in the section entitled "Statistical Comparison of Optimal robust Installation Designs".

Presented in Figure (37h) is a comparison of the mean of the first five Fourier harmonic 1/2 amplitudes of engine face distortion for the $\Delta X/c = 4.0$ and $\Delta X/c = 2.0$ configurations over the angle-of-incidence range from 0° to 20.0°. The results indicate that the optimal robust Maximum HCF Life Expectancy installation designs "collectively" reduced the first five Fourier harmonic 1/2 amplitudes of engine face distortion, and that low level can be maintained over the angle-of-incidence range from 0° to $20.0.^{\circ}$ Thus the robustness properties of micro-vane effector installations also extends to the Fourier harmonic 1/2 amplitudes of engine face distortion.

Comparison of the mean Fourier harmonic 1/2 amplitude for the optimal Robust Maximum Performance installation, Figure (24h), and the optimal Robust Maximum HCF Life expectancy installation, Figure (37h), indicates a "collective" lower mean Fourier harmonics 1/2 amplitude characteristics over the 0° to $20.0.^{\circ}$ angle-of-incidence range for the Maximum HCF Life Expectancy design. However, comparing the total pressure recovery characteristics for the same two optimal robust installation designs, Figure (24a) and Figure (37a), indicates that this improvement in HCF characteristics cost about 2.5 percent in total pressure recovery (PFAVE). It is presently not known whether the differences between the two respective optimal robust installations discussed would make any impact on engine maintainability. Not enough is presently known about High Cycle Fatigue to make that judgement. However, it has been demonstrated that an "open loop" robust micro-vane effector installation designs have the ability to maintain excellent total pressure recovery (PFAVE), the engine face distortion (DC60), and the first five Fourier harmonic 1/2 amplitudes of engine face distortion (Fi/2, i=1,5) characteristics over and angle-of-incidence range. The ability to develop such robust installation designs is a consequence of the factor interactions described in the section entitled "Micro-Vane effector Band Interactions". In order to successfully understand these interactions and put them together to achieve a design advantage requires a structured approach to design. That structured approach to MSFC design is satisfied by *Response Surface Methodologies*[3]-[4] and *Robustness Design Concepts.*[5]-[6]

Statistical Comparison of CFD Analysis and DOE Predictions

Extensive CFD validation cases were included in this study and these are presented in Tables (14) through (17) for both the $\Delta X/c = 4.0$ and $\Delta X/c = 2.0$ installation configurations. Table (14) defines the CFD validation installation geometries and flow conditions evaluated for the optimal Robust Maximum Performance installations at Reynolds numbers per ft. of 4.0×10^6, 12.0×10^6, and 20.0×10^6 each at 0^o angle of incidence in addition to angle-of-incidences of 0^o, 10.0^o, and 20.0^o each at a Reynolds number per ft. of 20.0×10^6. Table (15) contains a summary of the CFD results for each of the cases defined in Table (14). Likewise, Table (16) contains the the CFD validation installation geometries and flow conditions evaluated for the optimal Robust Maximum HCF Life Expectancy installations at the same flow conditions as in Table (14). Table (17) contains a summary of the CFD performance results for each of the ten validation cases defined in Table (16).

There are a total of 20 CFD validation cases. They represent the six optimal robust installation designs determined by the "Lower Order" Robust design methodology[5]. The CFD validation performance results for each of these 20 test cases included all the response variables important for this study, i.e. inlet pressure recovery (PFAVE), engine face distortion (DC60), and the first five Fourier harmonic 1/2 amplitudes of distortion (F1/2, F2/2, F3/2, F4/2, and F5/2). A direct statistical comparison can be made between the optimal responses predicted by the DOE models (Y_{DOE}) and the actual CFD predicted performance values (Y_{CFD}) through the expression:

$$t^* = \frac{\left|\ln(Y_{CFD}) - \ln(Y_{DOE})\right|}{\dfrac{\ln(Y_A) - \ln(Y_{DOE})}{t(0.975, N-p)}} \qquad (3)$$

where Y_A is the upper 95% confidence interval for the individual predicted response Y_{DOE} from the regression model, and t(0.975,N-p) is the 95% confidence t-value for N-p degrees of freedom. Since all the response parameters except for PFAVE were modelled using a natural log transformation, the natural log of the response (Y) had to be used, i.e. ln(Y), for those responses. For a statistically significant difference to exist between the DOE model predicted response (Y_{DOE}) and the CFD validation response prediction (Y_{CFD}), the expression:

$$t^* > t(0.975, N-p) \qquad (4)$$

must hold. Likewise, if the expression

$$t^* < t(0.975, N-p) \qquad (5)$$

is valid, the Y_{CFD} is not statistically different from Y_{DOE}. Therefore, for no significant statistical difference to exist between the DOE model predicted response Y_{DOE} and the CFD analysis response Y_{CFD}, the CFD response prediction must fall within the 95% confidence interval of the DOE model prediction for that response. In each case, the comparison was made with the optimal robust installation. See Tables (14) through (17). Tables (18) through (21) show the results of this

statistical comparison over the range of angle-of-incidences from 0° to 20.0° for the Maximum Performance and Maximum HCF Life Expectancy missions. In general, the number of incidences when the comparisons were statistically different was about 5%, which is remarkably good. This indicates that the CFD performance results are not statistically different from the DOE performance results (i.e. the CFD performance predictions fell within the 95% confidence interval of the DOE performance predictions). It also indicates that the optimal installations determined by the DOE models were a statistically valid optima when compared to the actual CFD installation analysis.

Statistical Comparison of DOE Band Spacing Regression Models

This section involves the statistical comparison of two DOE model predicted response values Y_i and Y_j from two different regression models (i) and (j) at two different optimal factor combinations X_i and X_j. The two DOE models were generated from the $\Delta X/c = 4.0$ and $\Delta X/c = 2.0$ set of cases represented by Tables (4) and (5). Again, since all the responses except PFAVE were conducted using a natural log transformation, all the responses (except PFAVE) were considered as $\ln(Y_i)$ and $\ln(Y_j)$. A direct statistical comparison can be made between the optimal response Y_i predicted by the DOE model (i) having optimal factor combinations X_i, with the response Y_j predicted by DOE model (j) having optimal factor combinations X_j through the expression:

$$t^* = \frac{\left|\ln(Y_i) - \ln(Y_j)\right|}{\sqrt{\left(\frac{\ln(Y_A) - \ln(Y_i)}{t(0.975, N-p)}\right)^2 + \left(\frac{\ln(Y_B) - \ln(Y_j)}{t(0.975, N-p)}\right)^2}} \qquad (6)$$

where Y_A is the upper 95% confidence interval for the individual response Y_i from DOE model (i), Y_B is the upper 95% confidence interval for the individual response Y_j from DOE model (j), and t(0.975,N-p) is the 95% confidence t-value for N-p degrees of freedom in error. For a statistically significant difference to exist between the DOE model (i) predicted response (Y_i) and the DOE model (j) predicted response (Y_j), the expression:

$$t^* > t(0.975, N-p) \qquad (7)$$

must be hold. Likewise, if the expression

$$t^* < t(0.975, N-p) \qquad (8)$$

is valid, the Y_i is not statistically different from Y_j. The statistical comparison between the DOE robust methodologies are presented is Tables (22) through (25), for both the Maximum Performance and Maximum HCF Life Expectancy missions. Statistical differences were found to exist in 5% to 7% of the comparisons. when comparing the DOE model from the $\Delta X/c = 4.0$ and $\Delta X/c = 2.0$ set of cases represented by Tables (4) and (5). This indicates that the performance results

between the two installation configurations were not statistically different. Although the inlet total pressure (PFAVE) comparisons of the two installation configurations from Figures (24a) and (37a) suggest that spacing the micro-vane effector bands closer together results in somewhat higher losses, this comparison indicates no significant statistical difference.

CONCLUSIONS

In the 1950s and 1960s, Box[3]-[4] and co-workers developed a collection of analytical and statistical experimental design tools for which the term *Response Surface Methodology* (RSM) was coined. RSM provides an economical, reliable and systematic approach to variable screening as well as the general exploration of the region that contains the estimated optimal conditions. One critical aspect of RSM is its ability to study statistical interactions among the design variables. These interactions often indicate a potential for achieving a robust installation design. A statistical interaction exists between two independent factor variables X_1 and X_2 when the effect of X_1 on response Y_i is affected by the value of X_2. In other words, the effect of factor X_1 on response Y_i is not unique, but changes as a function factor X_2. This is often called a synergistic effect, and it is very important in MSFC installation design.

The (h_2*h_3), (h_1*h_3), and (h1*h2) band interactions were such that no interactions occurred for the inlet total pressure recovery (PFAVE), while strong interactions resulted for the engine face distortion (DC60). The engine face distortion interaction was characterized by the behavior that when the "base" band heights (h_3) were set to 2.0 mm, the DC60 engine face distortion was not appreciable affected by increases in the micro-vane heights in the adjacent upstream installation bands. The natural aerodynamics characteristics of these installations of micro-vane effectors were such that once the vortices generated by the micro-vanes balanced the natural secondary flow in the inlet, (i.e. DC60 $\leq$ 0 10), the engine face distortion was not altered with further increases in installation band strength. With this factor interaction, it is possible to increase the "strength" of the installation bands to accommodate a stronger inlet secondary flow field resulting from a different mission condition without altering the performance at the original mission condition. Thus, this interaction for engine face distortion (DC60) indicated a potential for achieving a fixed robust installation design able to accommodate an angle-of-incidence variation without significantly effecting engine face distortion. The potential for achieving a truly robust installation design, able to achieve excellent performance over an angle-of-incidence range with a fixed micro-vane effector configuration, was realized by using optimal robustness techniques in conjunction with *Response Surface Methodologies*.

To illustrate the potential of *Response Surface Methodology* (RSM) and robustness considerations to design and optimize robust MSFC installations, two different mission strategies were considered for the subject inlet, namely (1) Maximum Performance, and (2) Maximum HCF Life Expectancy. The Maximum Performance mission sought to minimize the inlet duct losses (maximize the engine face total pressure recovery) subject to the constraint that the DC60 engine face distortion be less or equal to 0.10. This Maximum Performance mission placed no conditions on the first five Fourier harmonic 1/2 amplitudes of distortion. A DC60 distortion level of 0.10 is significant because it would be acceptable for a commercial engine application. The Maximum HCF Life Expectancy mission sought to minimize the mean of the first five Fourier harmonic 1/2 amplitudes, (i.e. collectively reduce all the Fourier harmonic 1/2 amplitudes of distortion).This

mission was also subject to the constraint that the DC60 engine face distortion be less than 0.10, but no constraint was placed upon the inlet total pressure recovery.

A comparison of the DOE performance differences between the optimal robust installation designs for the $\Delta X/c = 4.0$ and $\Delta X/c = 2.0$ configurations indicated that a near constant engine face distortion was achieved (i.e. DC60 ≤ 0.10) over the angle-of-incidence range from 0^{o} to 20.0^{o} for both the Maximum Performance and Maximum HCF Life Expectancy missions. The total pressure recovery (PFAVE) characteristics for all the optimal robust installation designs fell below the baseline flow solution. The also results indicated that both the optimal Robust Maximum HCF Life Expectancy installation designs "collectively" reduced the first five Fourier harmonic 1/2 amplitudes of engine face distortion, and that low level can be maintained over the angle-of-incidence range from 0^{o} to $20.0.^{o}$ Thus the robustness properties of micro-vane effector installations also extends to the Fourier harmonic 1/2 amplitudes of engine face distortion. The improvement in HCF characteristics for the Maximum HCF Life Expectancy designs cost about 0.21% in total pressure recovery (PFAVE) over the Maximum Performance installation designs. It is presently not known, however, whether the 4.7% reduction in the mean Fourier harmonic 1/2 amplitudes for the Maximum HCF Life Expectancy) would make any impact on engine maintainability. Not enough is presently known about High Cycle Fatigue to make that judgement. However, it has been demonstrated that an "open loop" robust micro-vane effector installation designs have the ability to maintain excellent total pressure recovery (PFAVE), the engine face distortion (DC60), and the first five Fourier harmonic 1/2 amplitudes of engine face distortion (Fi/2, i=1,5) characteristics over and angle-of-incidence range.

A statistical comparison of CFD analysis and DOE prediction indicates that the CFD performance results were not statistically different from the DOE performance results (i.e. the CFD performance predictions fell within the 95% confidence interval of the DOE performance predictions). This study indicated that the optimal installations determined by the DOE models were a statistically valid optima when compared to the actual CFD installation analysis. A statistical comparison of optimal robust installation designs indicates that the performance between the $\Delta X/c = 4.0$ and $\Delta X/c = 2.0$ configurations, for both the Maximum Performance and Maximum HCF Life Expectancy mission strategies, were not statistically different. Although the inlet total pressure (PFAVE) comparisons of the two installation configurations suggest that spacing the micro-vane effector bands closer together results in somewhat higher losses, this was not supported by a statistical comparison of the $\Delta X/c = 4.0$ and $\Delta X/c = 2.0$ DOE models. In other words, no performance penalty could be statistically established as a result of compressing the band spacing to within one chord length of each other, i.e. $\Delta X/c = 2.0$.

The ability to develop such robust installation designs is a consequence of the factor interactions described in the section entitled "Micro-Vane effector Band Interactions". In order to successfully understand these interactions and put them together to achieve a design advantage requires a structured approach to design. That structured approach to MSFC design is satisfied by *Response Surface Methodologies* and robustness techniques.

REFERENCES

(1) Anderson, B. H., Miller, D. N., Yagle, P. J, and Truax, P. P., "A Study of MEMS Flow Control for the Management of Engine Face Distortion in Compact Inlet Systems", FEDSM99-6920, 3rd ASME/JSME Joint Fluids Engineering Conference, San Francisco, CA, July 18-23, 1999.

(2) Hamstra, J. W., Miller, D. N., Truax, P. P., Anderson, B. H., and Wendt, B. J., "Active Inlet Flow Control Technology Demonstration," ICAS-2000-6.11.2, 22nd International Congress of the Aeronautical Sciences, Harrogate, UK, August 27th-September 1st, 2000.

(3) Box, G. E. P., and Jones, S., "*Empirical Model Building and Response Surfaces*," John Wiley, New York, 1987

(4) Box, G. E. P., Hunter, W. G., and Hunter, J. S., "*Statistics for Experimenters*," John Wiley, New York, 1978.

(5) Anderson, B. H. Keller, D. J., "A Parameter Design Methodology for Micro-Scale Secondary Flow Control in Compact Inlets," AIAA Paper No. 2002-0541, Jan. 2002

(6) Anderson, B. H. Keller, D. J., "Robust Parameter Design Methodologies for Micro-Scale Secondary Flow Control in Compact Inlets,"NASA TM, 2002-211477, March 2002.

(7) Anderson, B. H., Keller, D. J., "Considerations in the Measurement of Inlet Distortion For High Cycle Fatigue in Compact Inlet Diffusers", NASA TM, 2002-211476, March 2002.

(8) Willmer, A. C., Brown, T. W. and Goldsmith, E. L., "Effects of Intake Geometry on Circular Pitot Intake Performance at Zero and Low Forward Speeds", Aerodynamics of Power Plant Installation, AGARD CP301, Paper 5, Toulouse, France, May 1981, pp 51-56.

(9) Bender, E. E, Anderson, B. H., and Yagle, P. J., "Vortex Generator Modeling for Navier Stokes Code", FEDSM99-69219, 3rd ASME/JSME Joint Fluids Engineering Conference, San Francisco, CA, July 18-23, 1999.

(10) Gibb, J. and Anderson, B. H., "Vortex Flow Control Applied to Aircraft Intake Ducts," Proceedings of the Royal Aeronautical Society Conf., High Lift and Separation Control, Paper No. 14, Bath, UK, March, 1995.

(11)Ludwig, G. R., "Aeroelastic Considerations in the Measurement of Inlet Distortion," 3rd National Turbine Engine High Cycle Fatigue Conference, 1998.

(12) Goldsmith, E. L., and Seddon, J. (eds), "Practical Intake Aerodynamics," Blackwell Scientific Publications, Oxford, 1993.

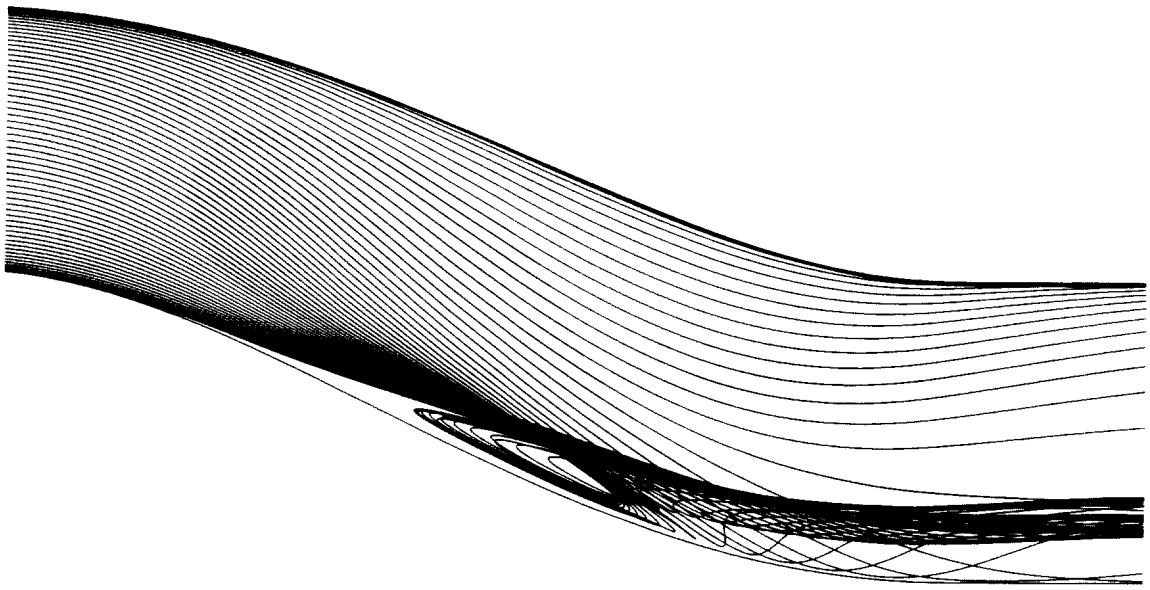

Figure (1): Particles traces showing the vortex liftoff (separation) within the DERA/M2129 inlet S-duct, Mt = 0.70, Re = 20.0 x 10^6/ft., α = 0.0°.

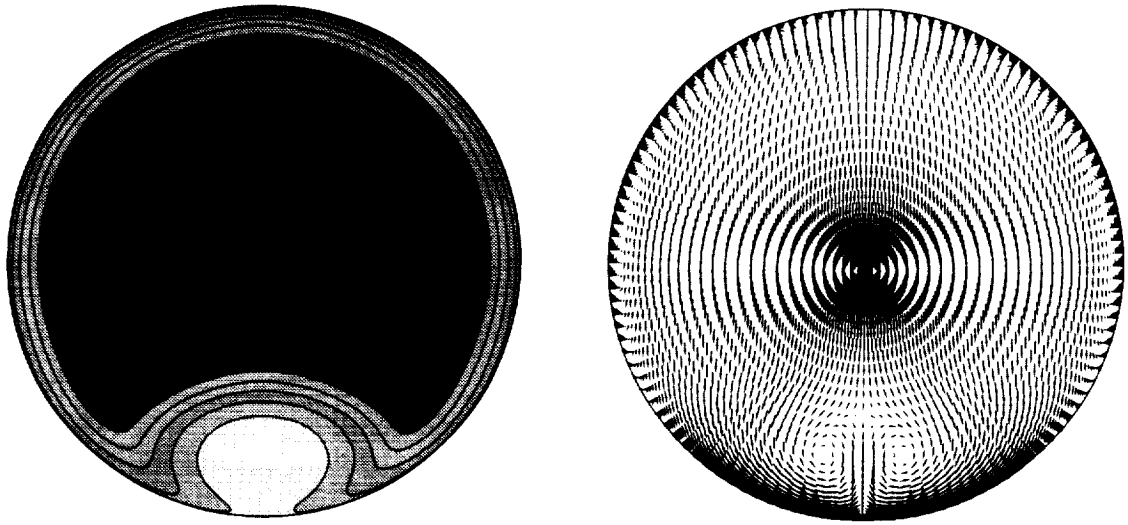

(a) Total Pressure Recovery Contours **(b) Secondary Flow Velocity Vectors**

Figure (2): Baseline engine face solution, Mt = 0.70, Re = 20.0 x 10^6/ft., α = 0.0°.

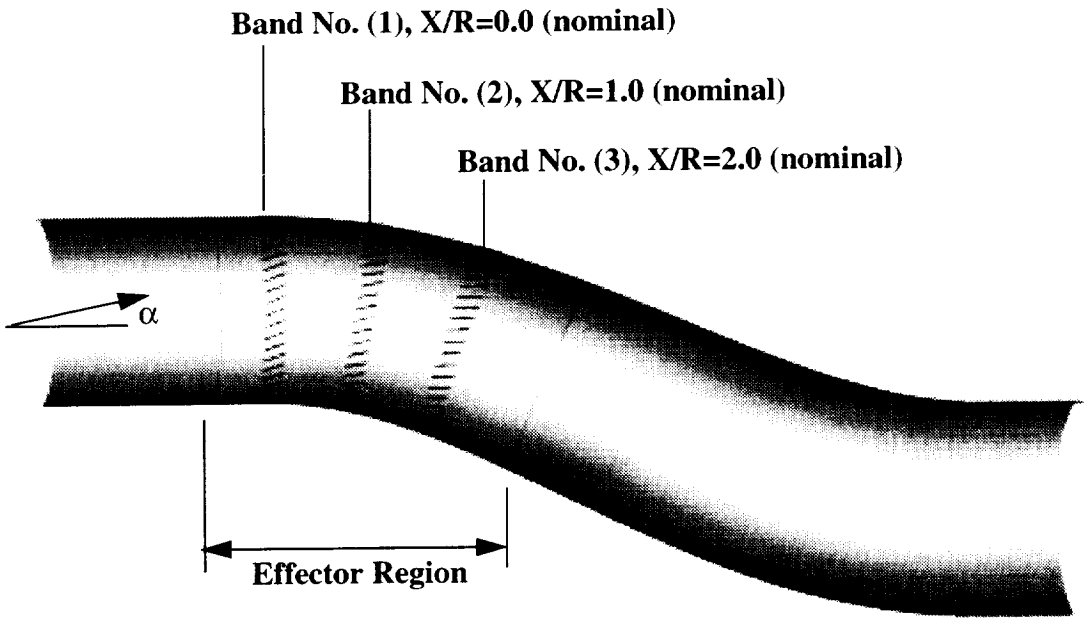

Figure (3): Location of effector region within the DERA/M2129 inlet S-duct for DOE study, ΔX/c = 4.0.

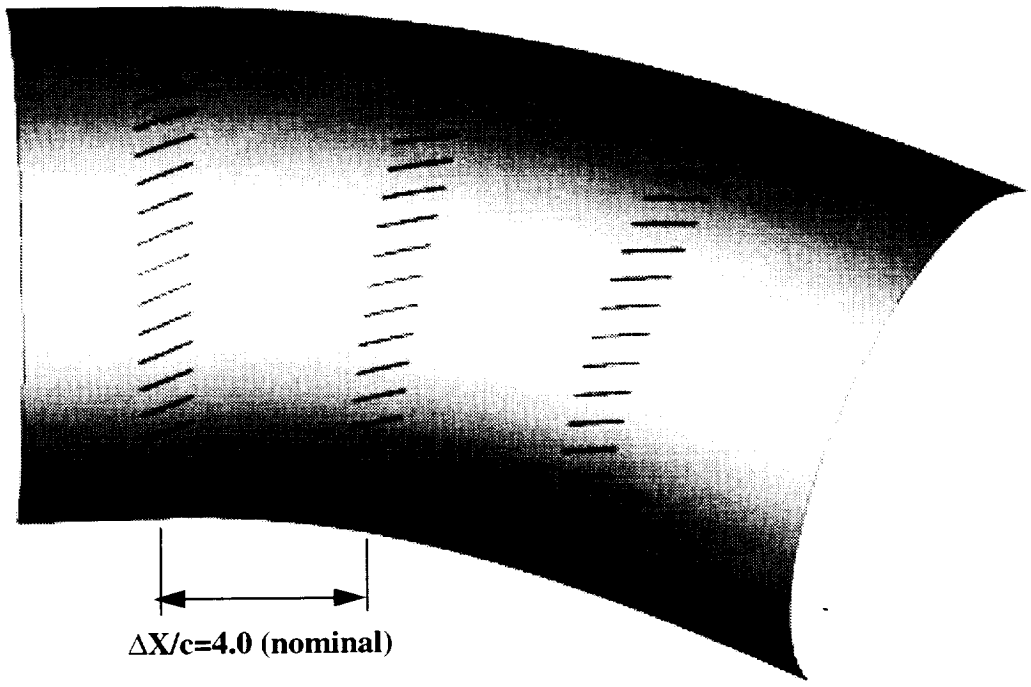

Figure (4): Micro-vane effector arrangement within effector region for DOE study, ΔX/c = 4.0.

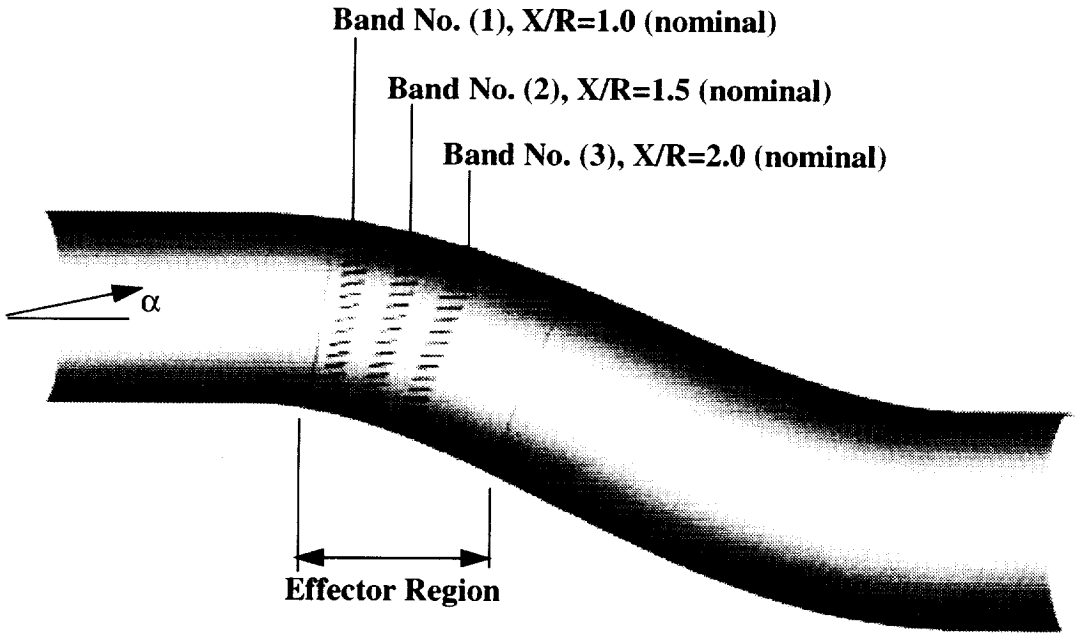

Figure (5): Location of effector region within the DERA/M2129 inlet S-duct for DOE, ΔX/c = 2.0.

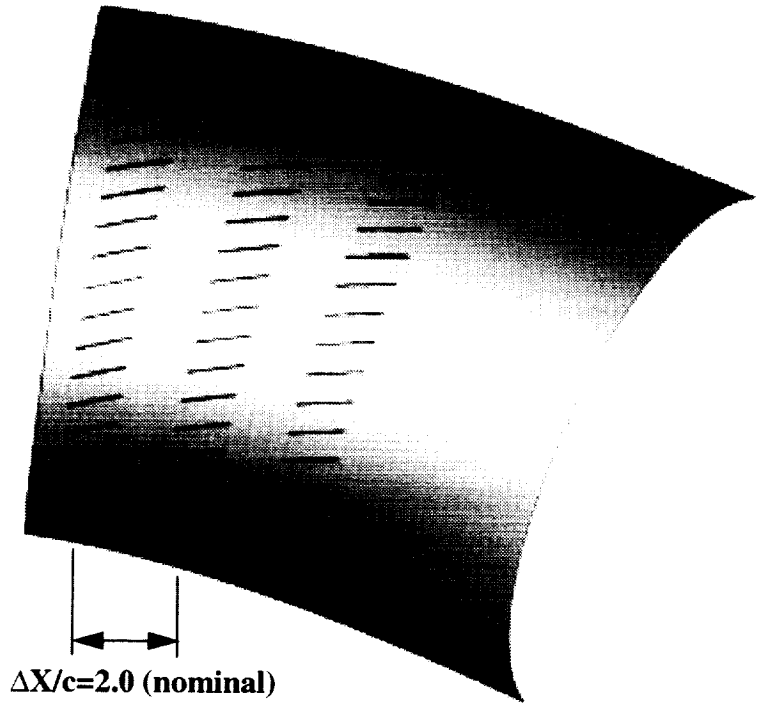

Figure (6): Micro-vane effector arrangement within effector region for DOE study, ΔX/c = 2.0.

Factors	Range
First Installation Micro-Vane Heights (mm), h_1	0.0 to 2.0
Second Installation Micro-Vane Heights (mm), h_2	0.0 to 2.0
Third Installation Micro-Vane Heights (mm), h_3	0.0 to 2.0
Inlet Angle-of-Incidence, (degs.), α	0.0^o to 20.0^o
Reynolds Number per ft. Re	$4.0x10^6$ to $20.0x10^6$

Table (1): Factors which establish the DOE design matrix.

Variable	Value
Number of Effector Units, $n_{i,\ i=1,3}$	24
Micro-Vane Angle-of-Incidence, (degs.), $\beta_{i,\ i=1,3}$	24.0^o
Installation Micro-Vane Chord Length (mm), $c_{i,\ i=1,3}$	16.0
Throat Mach Number, Mt	0.700
Inlet Angle-of-Yaw, (degs.), γ	0.0^o

Table (2): Variables held constant

Design Responses	Nomenclature
Engine Face Total Pressure Recovery	PFAVE
Engine Face Distortion	DC60
1st Fourier Harmonic 1/2 Amplitude	F1/2
2nd Fourier Harmonic 1/2 Amplitude	F2/2
3rd Fourier Harmonic 1/2 Amplitude	F3/2
4th Fourier Harmonic 1/2 Amplitude	F4/2
5th Fourier Harmonic 1/2 Amplitude	F5/2

Table (3): DOE design responses

Config.	h_1	h_2	h_3	α	Re
nvg701	0.0	0.0	0.0	0.0	20.0
nvg702	2.0	0.0	0.0	0.0	4.00
nvg703	0.0	2.0	0.0	0.0	4.00
nvg704	2.0	2.0	0.0	0.0	20.0
nvg705	0.0	0.0	2.0	0.0	4.00
nvg706	2.0	0.0	2.0	0.0	20.0
nvg707	0.0	2.0	2.0	0.0	20.0
nvg708	2.0	2.0	2.0	0.0	4.00
nvg709	0.0	0.0	0.0	20.0	4.00
nvg710	2.0	0.0	0.0	20.0	20.0
nvg711	0.0	2.0	0.0	20.0	20.0
nvg712	2.0	2.0	0.0	20.0	4.00
nvg713	0.0	0.0	2.0	20.0	20.0
nvg714	2.0	0.0	2.0	20.0	4.00
nvg715	0.0	2.0	2.0	20.0	4.00
nvg716	2.0	2.0	2.0	20.0	20.0
nvg717	0.0	1.0	1.0	10.0	12.0
nvg718	2.0	1.0	1.0	10.0	12.0
nvg719	1.0	0.0	1.0	10.0	12.0
nvg720	1.0	2.0	1.0	10.0	12.0
nvg721	1.0	1.0	0.0	10.0	12.0
nvg722	1.0	1.0	2.0	10.0	12.0
nvg723	1.0	1.0	1.0	0.0	12.0
nvg724	1.0	1.0	1.0	20.0	12.0
nvg725	1.0	1.0	1.0	10.0	4.00
nvg726	1.0	1.0	1.0	10.0	20.0
nvg727	1.0	1.0	1.0	10.0	12.0

Table (4): Central Composite Face-Centered (CCF) DOE, $\Delta X/c = 4.0$

Config.	h_1	h_2	h_3	α	Re
nvg801	0.0	0.0	0.0	0.0	20.0
nvg802	2.0	0.0	0.0	0.0	4.00
nvg803	0.0	2.0	0.0	0.0	4.00
nvg804	2.0	2.0	0.0	0.0	20.0
nvg805	0.0	0.0	2.0	0.0	4.00
nvg806	2.0	0.0	2.0	0.0	20.0
nvg807	0.0	2.0	2.0	0.0	20.0
nvg808	2.0	2.0	2.0	0.0	4.00
nvg809	0.0	0.0	0.0	20.0	4.00
nvg810	2.0	0.0	0.0	20.0	20.0
nvg811	0.0	2.0	0.0	20.0	20.0
nvg812	2.0	2.0	0.0	20.0	4.00
nvg813	0.0	0.0	2.0	20.0	20.0
nvg814	2.0	0.0	2.0	20.0	4.00
nvg815	0.0	2.0	2.0	20.0	4.00
nvg816	2.0	2.0	2.0	20.0	20.0
nvg817	0.0	1.0	1.0	10.0	12.0
nvg818	2.0	1.0	1.0	10.0	12.0
nvg819	1.0	0.0	1.0	10.0	12.0
nvg820	1.0	2.0	1.0	10.0	12.0
nvg821	1.0	1.0	0.0	10.0	12.0
nvg822	1.0	1.0	2.0	10.0	12.0
nvg823	1.0	1.0	1.0	0.0	12.0
nvg824	1.0	1.0	1.0	20.0	12.0
nvg825	1.0	1.0	1.0	10.0	4.00
nvg826	1.0	1.0	1.0	10.0	20.0
nvg827	1.0	1.0	1.0	10.0	12.0

Table (5): Central Composite Face-Centered (CCF) DOE, $\Delta X/c = 2.0$

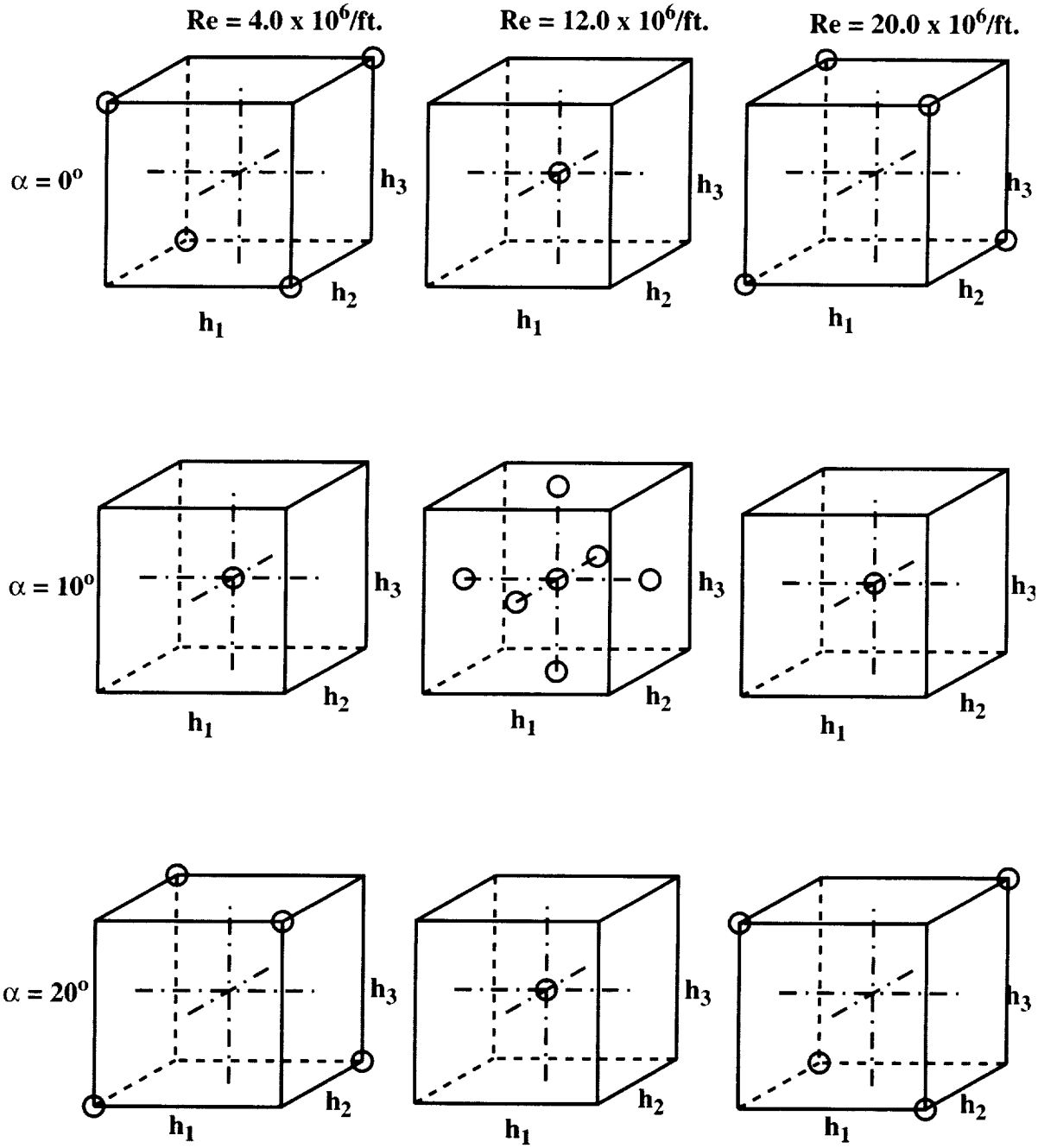

Figure (7): Graphical representation of Central Composite Face-Centered (CCF) DOE for both ΔX/c = 4.0, and ΔX/c = 2.0.

Ring Number	Radial Weighting Coefficient
1	0.05651
2	0.14248
3	0.21077
4	0.26918
5	0.32106

Table (6): Radial weighting coefficients applied to the total pressure rake measurements.

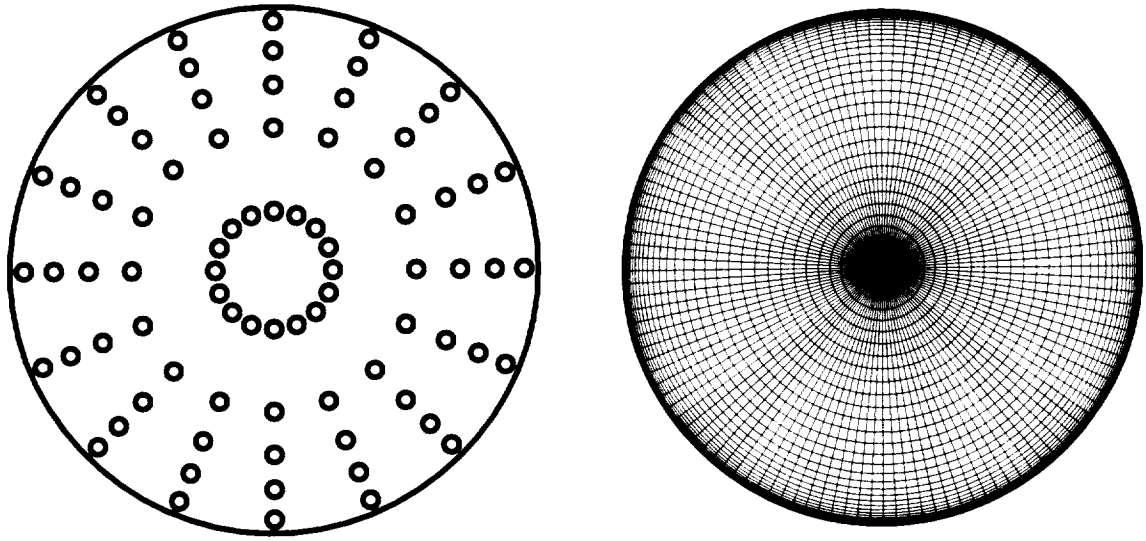

(a) 80-probe rake **(b) Computational grid**

Figure (8): Total pressure and distortion measurement arrays.

Response	Nomenclature	S^2_{max}/S^2_{min}	t(0.95,9,9)
1st Harmonic 1/2 Amplitude	F1/2	1002.4	4.03
2nd Harmonic 1/2 Amplitude	F2/2	47.2	4.03
3rd Harmonic 1/2 Amplitude	F3/2	93.8	4.03
4th Harmonic 1/2 Amplitude	F4/2	33.9	4.03
5th Harmonic 1/2 Amplitude	F5/2	40.6	4.03

Table (7): Fourier Harmonic 1/2 amplitude F-test compliance.

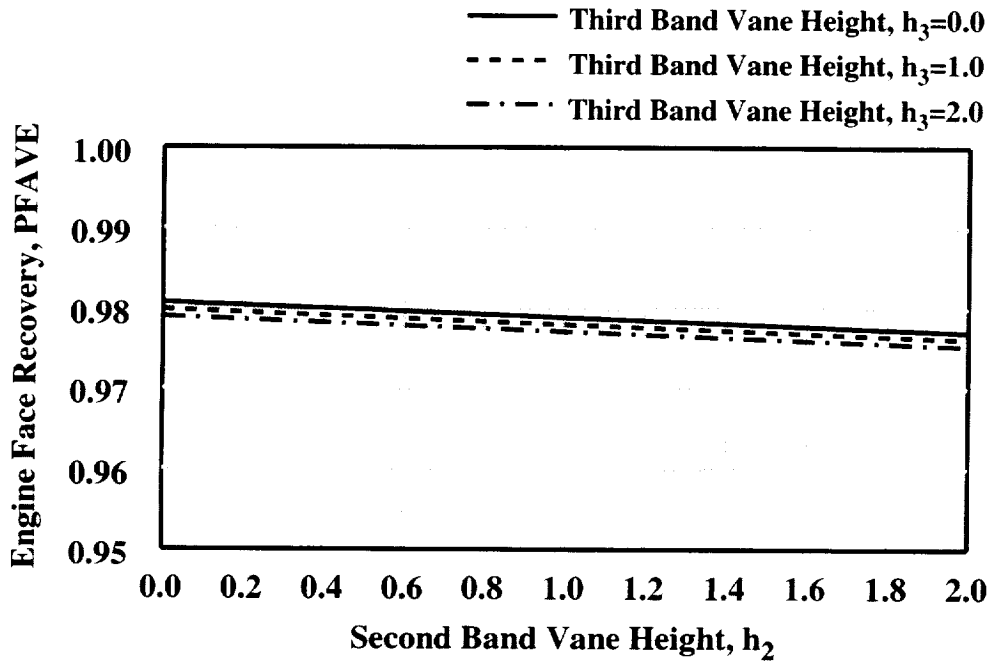

(a) Total Pressure Recovery Characteristics, $\Delta X/c = 4.0$

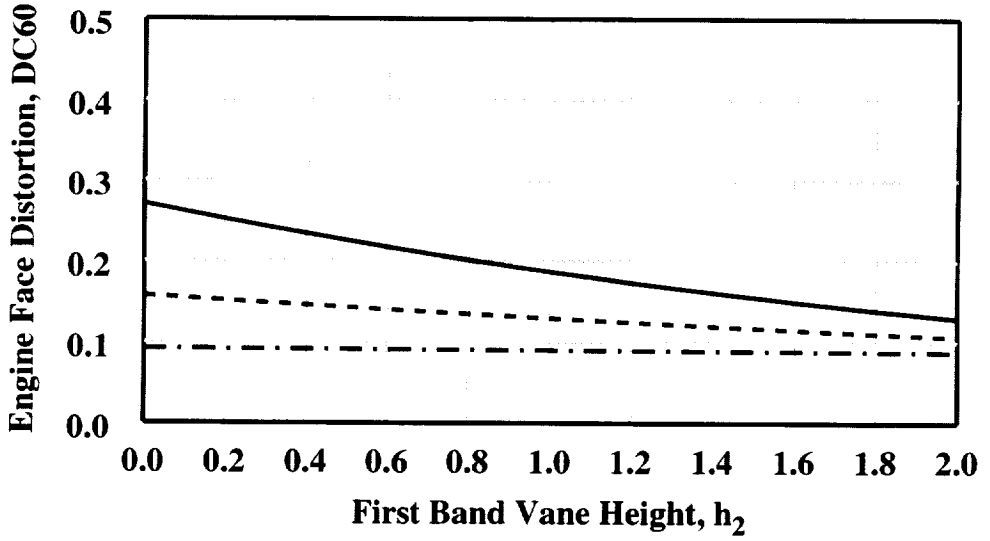

(b) Engine Face DC60 Distortion Characteristics, $\Delta X/c = 4.0$

Figure (9): Effect of the (h2*h3) micro-vane band interaction on inlet performance, $h_1 = 0.0$, Re = 20.0 x 10^6/ft., $\alpha = 0.0^o$.

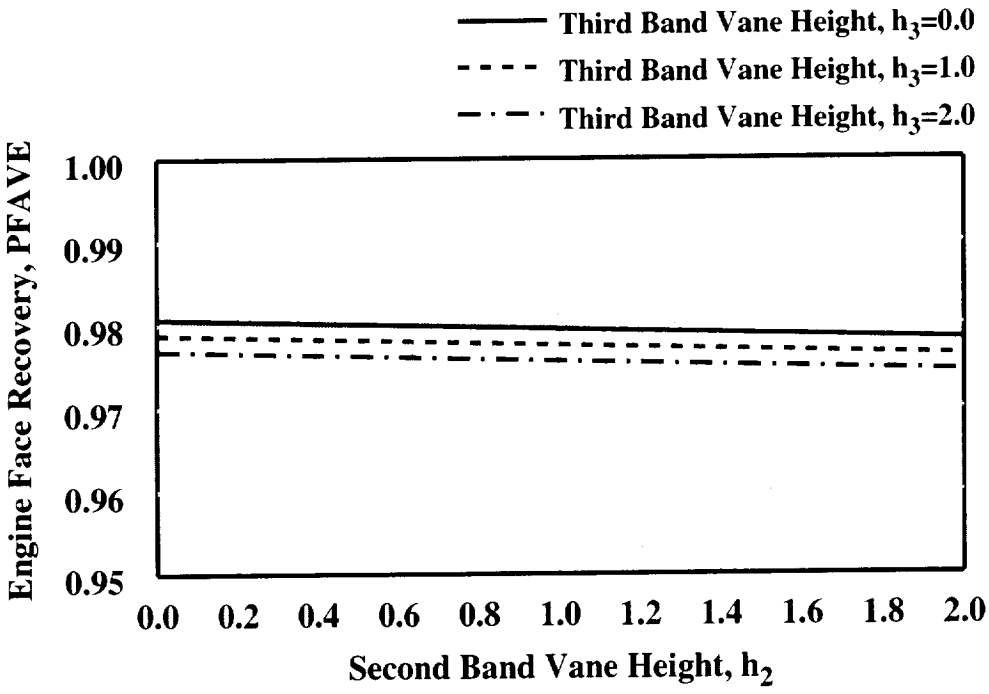

(c) Total Pressure Recovery Characteristics, $\Delta X/c = 2.0$

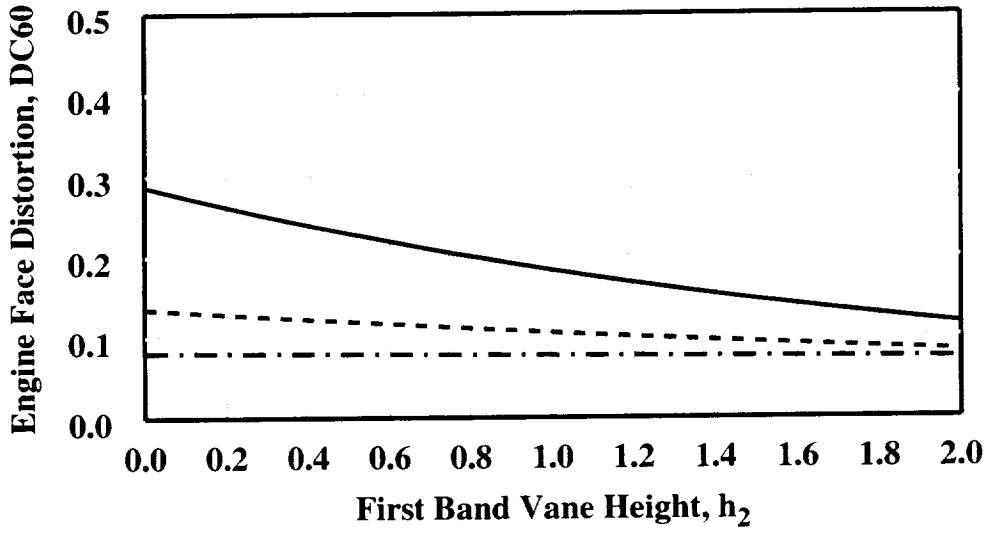

(d) Engine Face DC60 Distortion Characteristics,$\Delta X/c = 2.0$

Figure (9): Effect of the (h2*h3) micro-vane band interaction on inlet performance, $h_1 = 0.0$, Re = 20.0 x 10^6/ft., $\alpha = 0.0^o$.

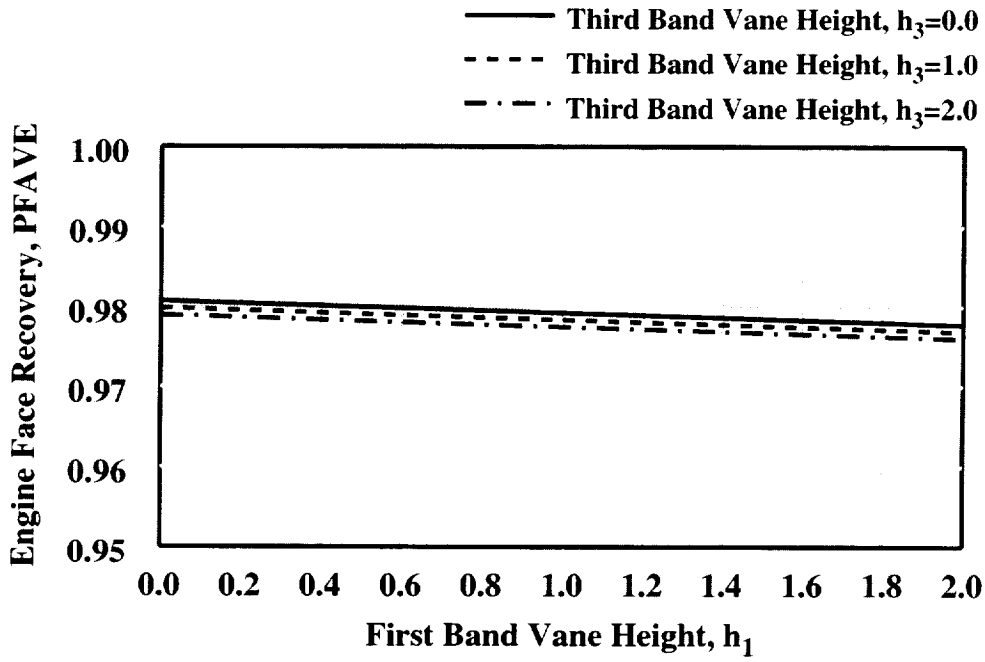

(a) Total Pressure Recovery Characteristics, $\Delta X/c = 4.0$

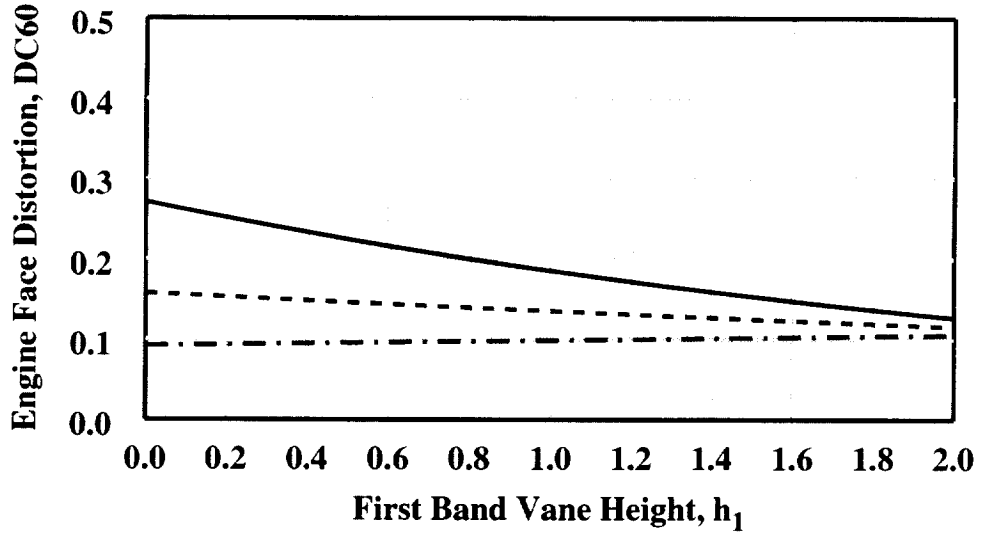

(b) Engine Face DC60 Distortion Characteristics, $\Delta X/c = 4.0$

Figure (10): Effect of the (h1*h3) micro-vane band interaction on inlet performance, $h_2 = 0.0$, Re = 20.0 x 10^6/ft., $\alpha = 0.0^o$.

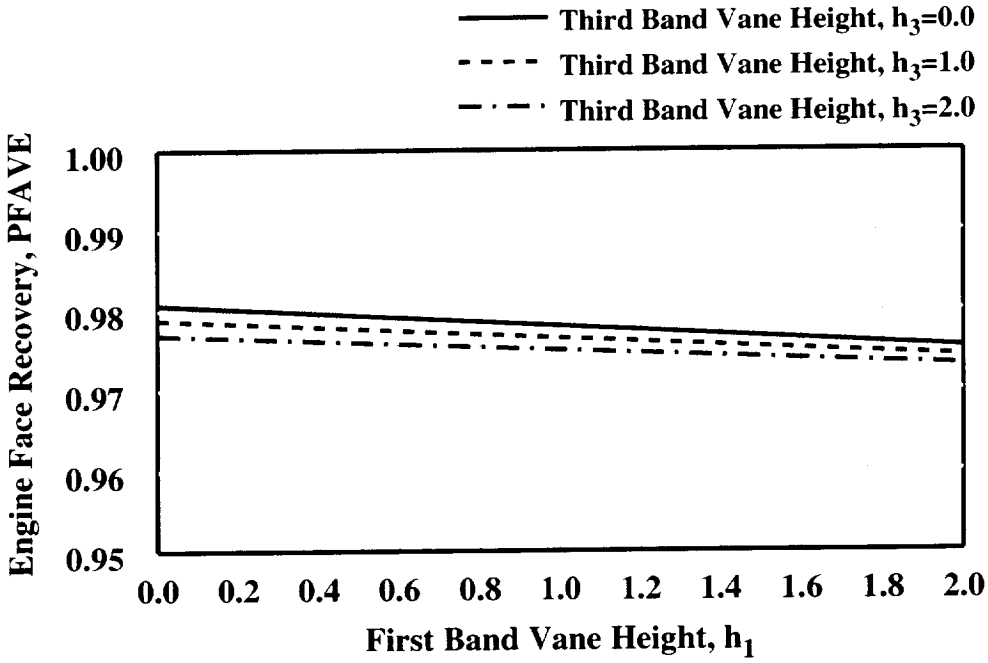

(c) Total Pressure Recovery Characteristics, $\Delta X/c = 2.0$

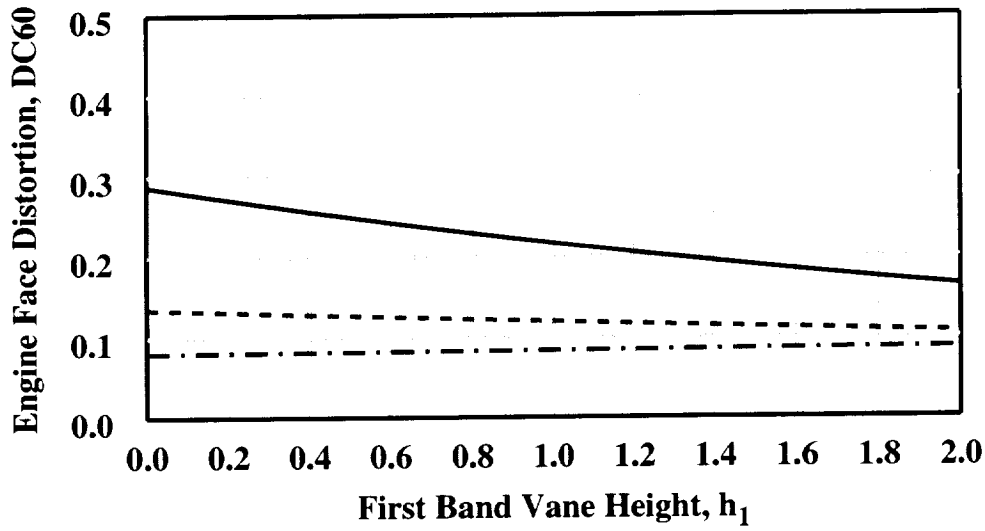

(d) Engine Face DC60 Distortion Characteristics, $\Delta X/c = 2.0$

Figure (10): Effect of the (h1*h3) micro-vane band interaction on inlet performance, $h_2 = 0.0$, Re = 20.0 x 10^6/ft., $\alpha = 0.0^o$.

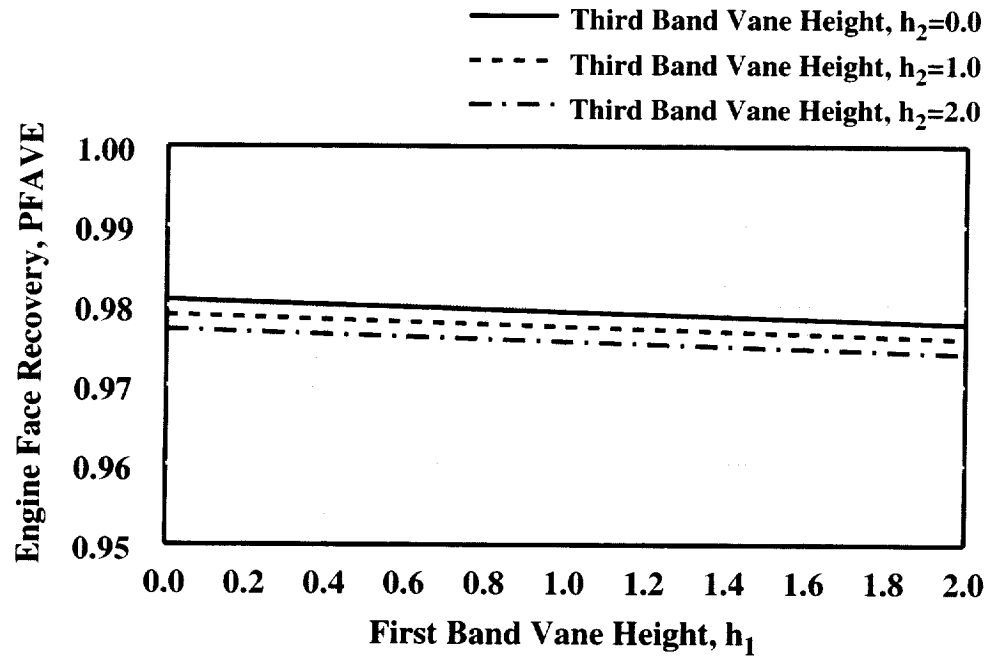

(a) Total Pressure Recovery Characteristics, $\Delta X/c = 4.0$

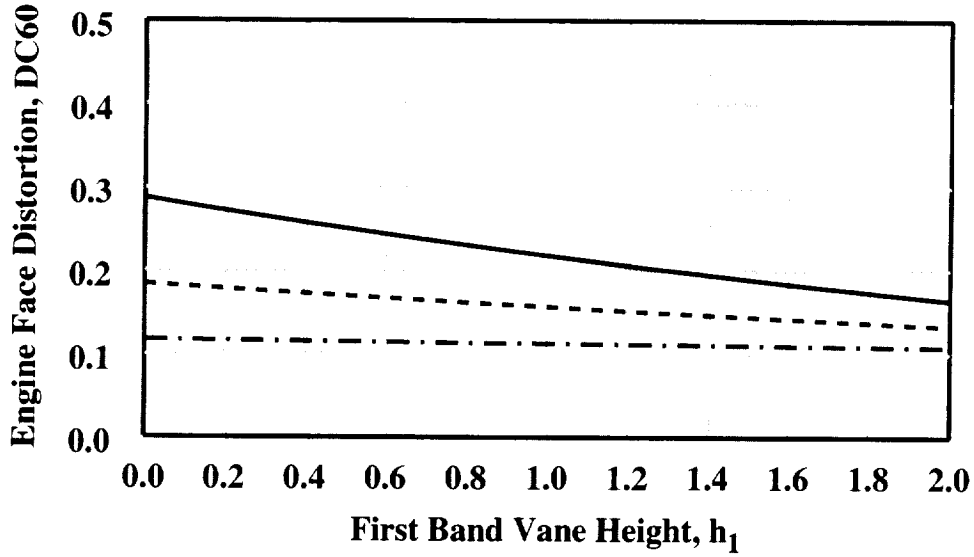

(b) Engine Face DC60 Distortion Characteristics, $\Delta X/c = 4.0$

Figure (11): Effect of the (h1*h2) micro-vane band interaction on inlet performance, $h_3 = 0.0$, Re = 20.0 x 10^6/ft., $\alpha = 0.0^o$.

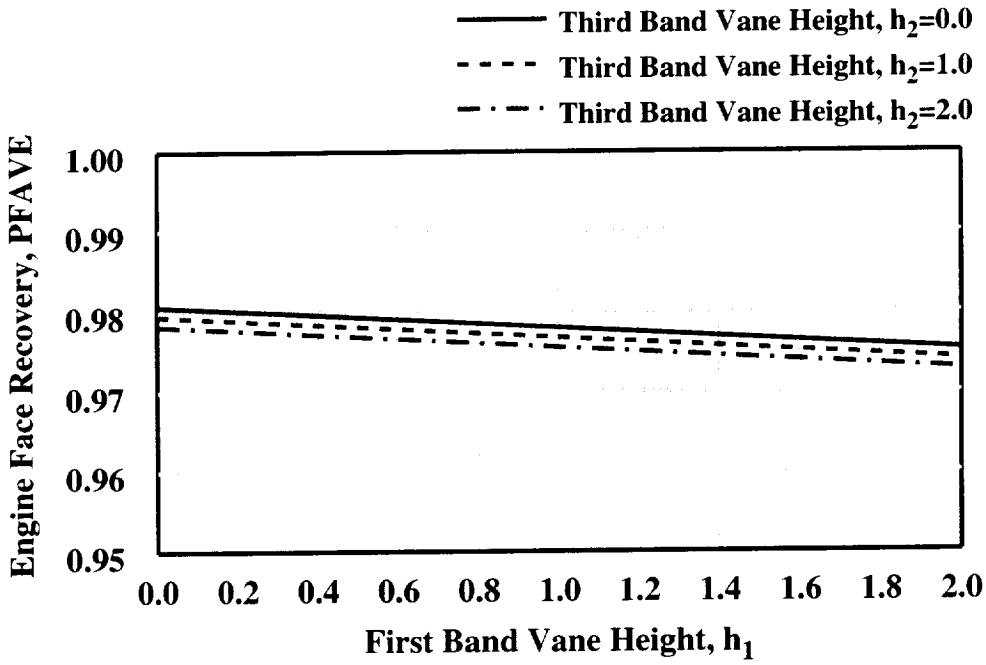

(c) Total Pressure Recovery Characteristics, $\Delta X/c = 2.0$

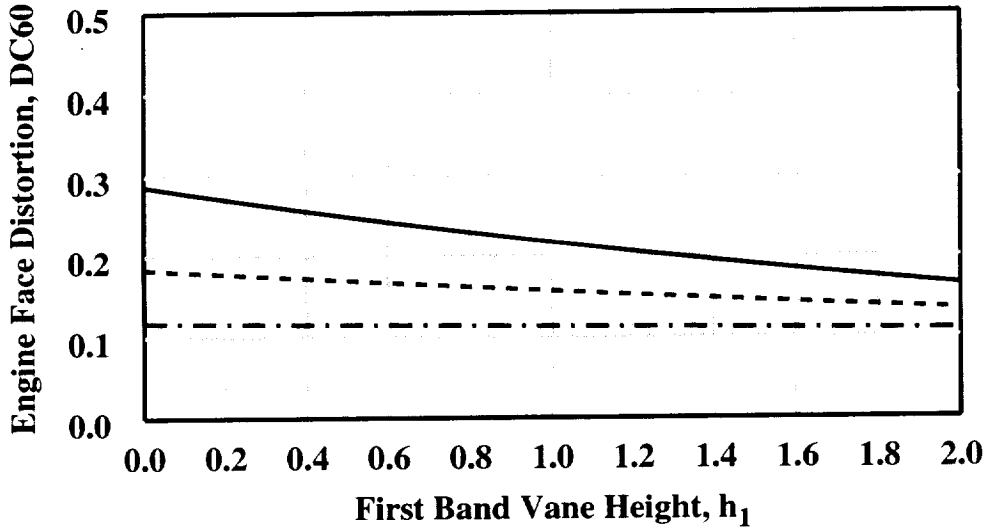

(d) Engine Face DC60 Distortion Characteristics, $\Delta X/c = 2.0$

Figure (11): Effect of the (h1*h2) micro-vane band interaction on inlet performance, h_3 = 0.0, Re = 20.0 x 10^6/ft., $\alpha = 0.0^o$.

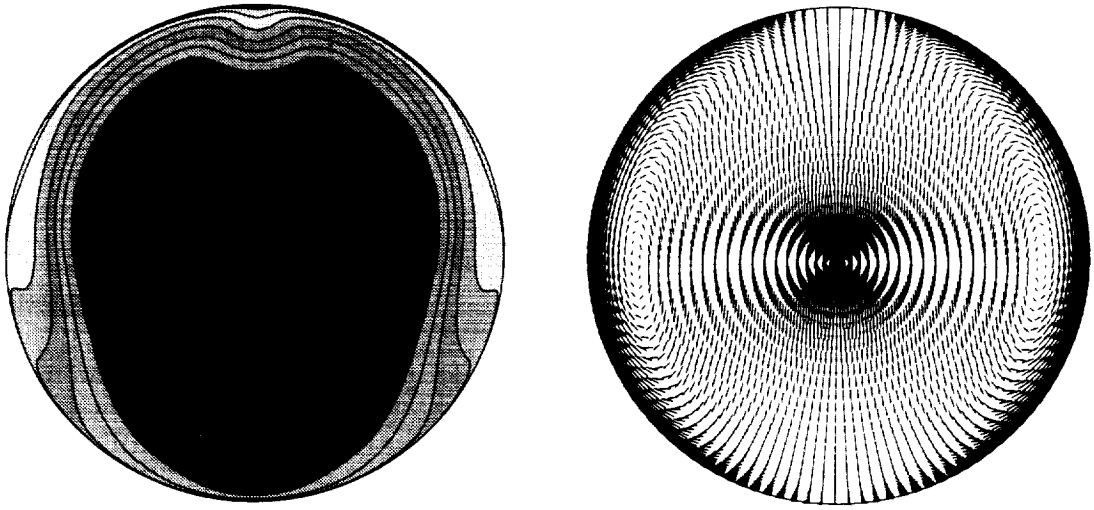

(a) Total Pressure Recovery (b) Secondary Flow Velocity

Figure (12): Optimal Robust Maximum Performance installation engine face CFD solution, $\Delta X/c = 4.0$, Re = 20.0 x 10^6/ft., $\alpha = 0.0^o$.

Factor/Response	Range/Constraint	Optimal Value
h_1	0.0 to 2.0	0.0
h_2	0.0 to 2.0	0.0
h_3	0.0 to 2.0	1.9
PFAVE	Maximized	0.98021
DC60	≤ 0.10	0.06929
F1/2	Unconstrained	0.01472
F2/2	Unconstrained	0.01439
F3/2	Unconstrained	0.00860
F4/2	Unconstrained	0.00561
F5/2	Unconstrained	0.00148

Table (10): Optimal Robust Maximum Performance installation inlet CFD performance, $\Delta X/c = 4.0$, Re = 20.0 x 10^6/ft., $\alpha = 0.0^o$.

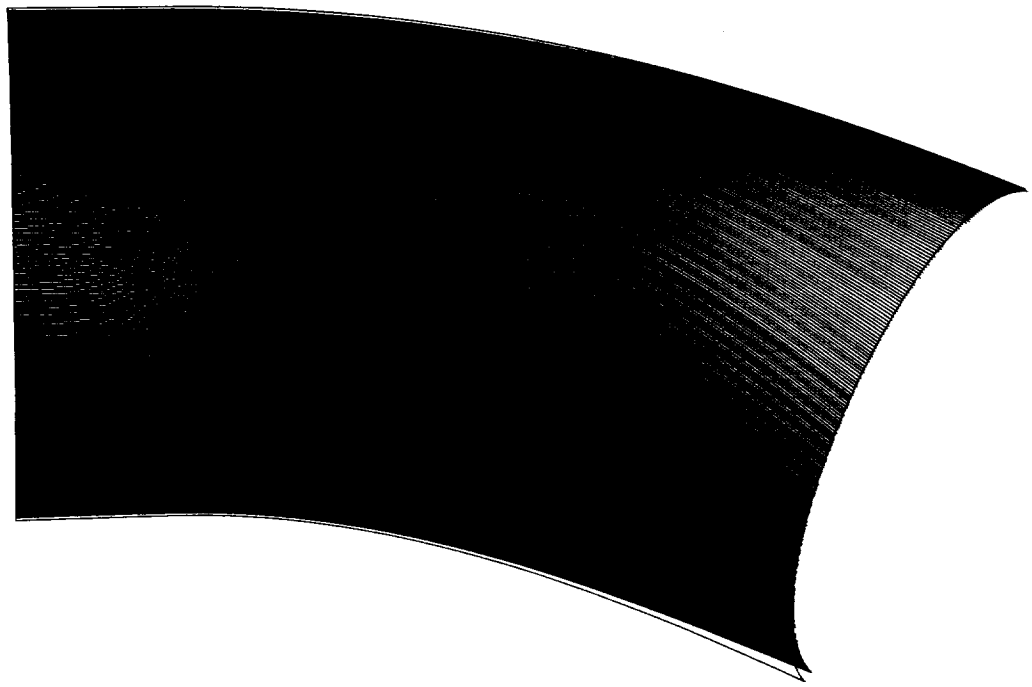

Figure(13): Near wall streamlines within effector region, baseline CFD solutions, Re = 20.0 x 10^6/ft., $\alpha = 0.0^o$.

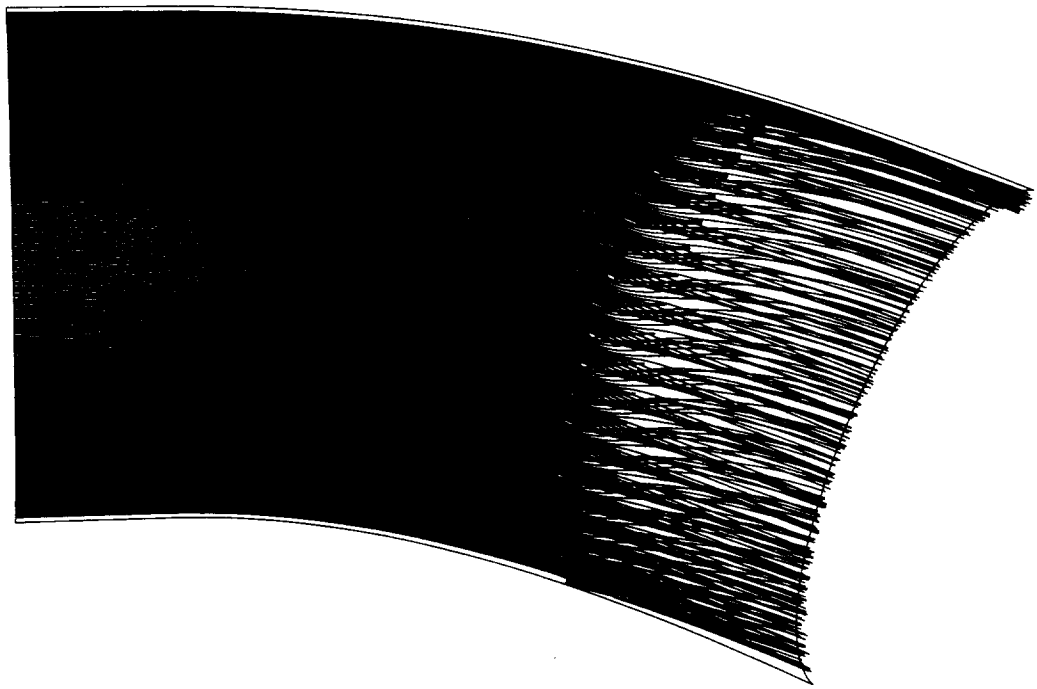

Figure (14): Near wall streamlines, Optimal Robust Maximum Performance installation design, $\Delta X/c = 4.0$, Re =20.0 x 10^6/ft., $\alpha = 0.0^o$.

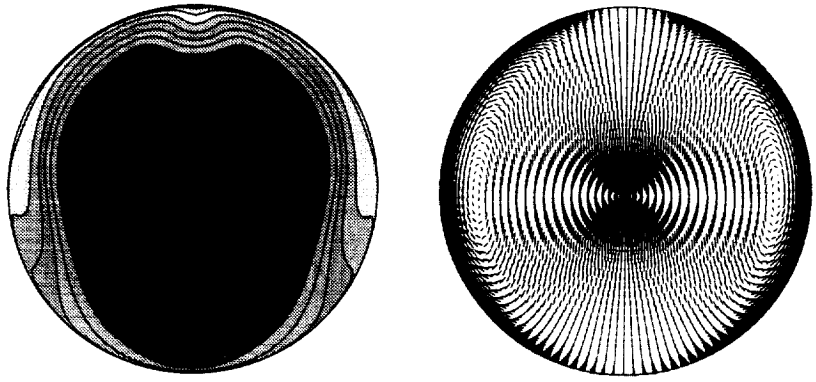

(a) Total PressureRecovery (b) Secondary Flow Velocity

Figure (15): Optimal Robust Maximum Performance installation engine face CFD solution, $\Delta X/c = 4.0$, Re = 20.0 x 10^6/ft., $\alpha = 0.0^o$.

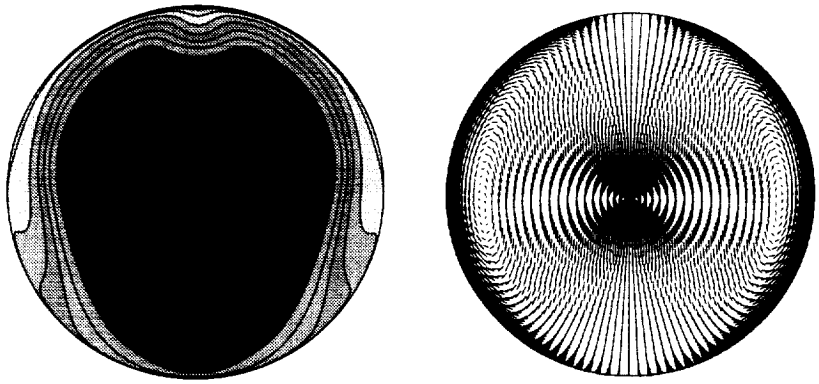

(a) Total Pressure Recovery (b) Secondary Flow Velocity

Figure (16): Optimal Robust Maximum Performance installation engine face CFD solution, $\Delta X/c = 4.0$, Re = 20.0 x 10^6/ft., $\alpha = 10.0^o$.

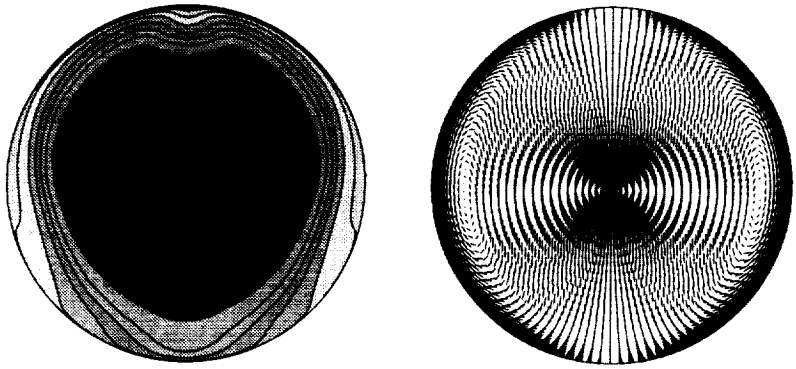

(a) Total Pressure Recovery (b) Secondary Flow Velocity

Figure (17): Optimal Robust Maximum Performance installation engine face CFD solution, $\Delta X/c = 4.0$, Re = 20.0 x 10^6/ft., $\alpha = 20.0^o$.

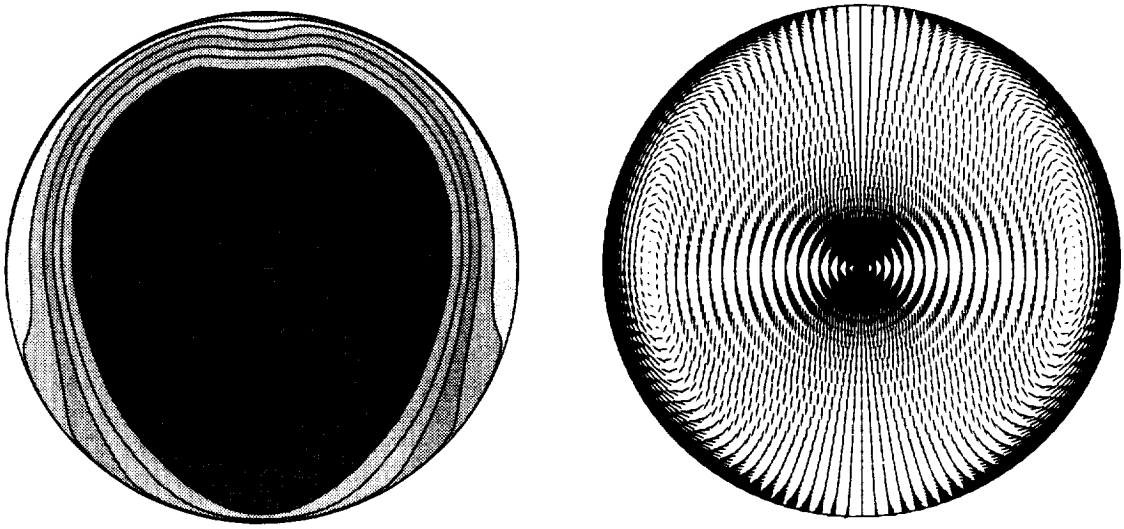

(a) Total Pressure Recovery (b) Secondary Flow Velocity

Figure (18): Optimal Robust Maximum Performance installation engine face CFD solution $\Delta X/c = 2.0$, Re = 20.0 x 10^6/ft., $\alpha = 0.0^o$.

Factor/Response	Range/Constraint	Optimal Value
h_1	0.0 to 2.0	0.0
h_2	0.0 to 2.0	0.10
h_3	0.0 to 2.0	1.50
PFAVE	Maximized	0.97794
DC60	≤ 0.10	0.06756
F1/2	Unconstrained	0.00903
F2/2	Unconstrained	0.01512
F3/2	Unconstrained	0.00906
F4/2	Unconstrained	0.00499
F5/2	Unconstrained	0.00177

Table (11): Optimal Robust Maximum Performance installation inlet CFD performance, $\Delta X/c = 2.0$, Re = 20.0 x 10^6/ft., $\alpha = 0.0^o$.

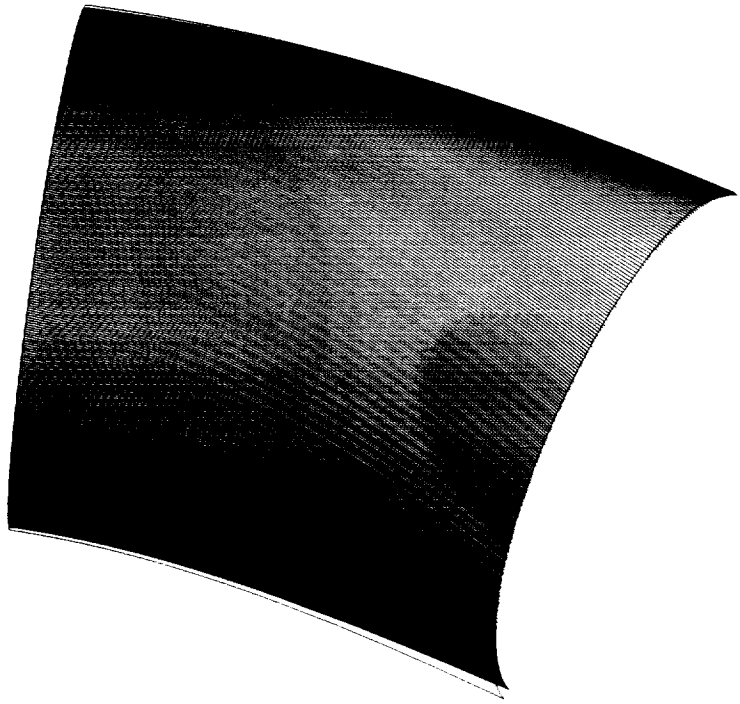

Figure (19): Near wall streamlines within effector region, baseline CFD solution, Re = 20.0 x 10^6/ft., $\alpha = 0.0^o$.

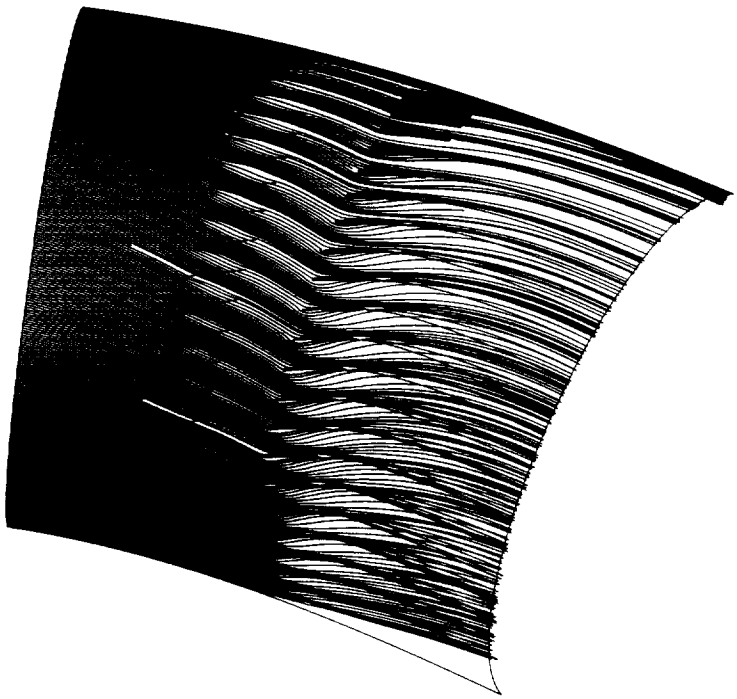

Figure (20): Near wall streamlines, Optimal Robust Maximum PerformanceCFD solution, $\Delta X/c = 2.0$, Re = 20.0 x 10^6/ft., $\alpha = 0.0^o$.

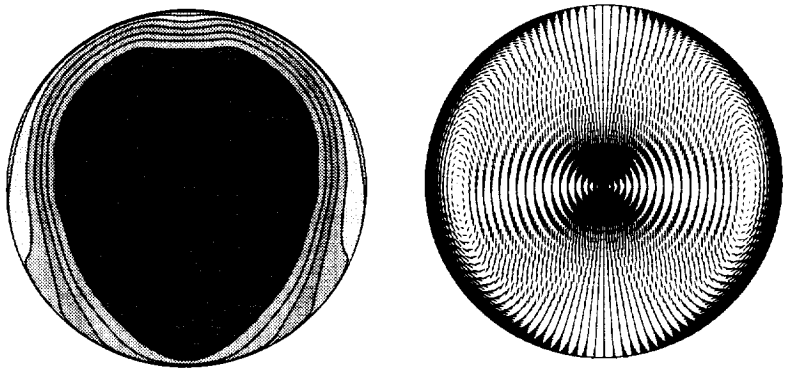

(a) Total Pressure Recovery (b) Secondary Flow Velocity

Figure (21): Optimal Robust Maximum Performance installation engine face CFD solution, $\Delta X/c = 2.0$, Re = 20.0 x 10^6/ft., $\alpha = 0.0^o$.

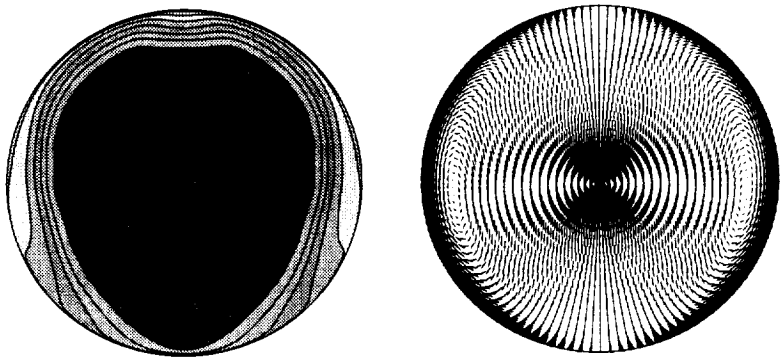

(a) Total Pressure Recovery (b) Secondary Flow Velocity

Figure (22): Optimal Robust Maximum Performance installation engine face CFD solution, $\Delta X/c = 2.0$, Re = 20.0 x 10^6/ft., $\alpha = 10.0^o$.

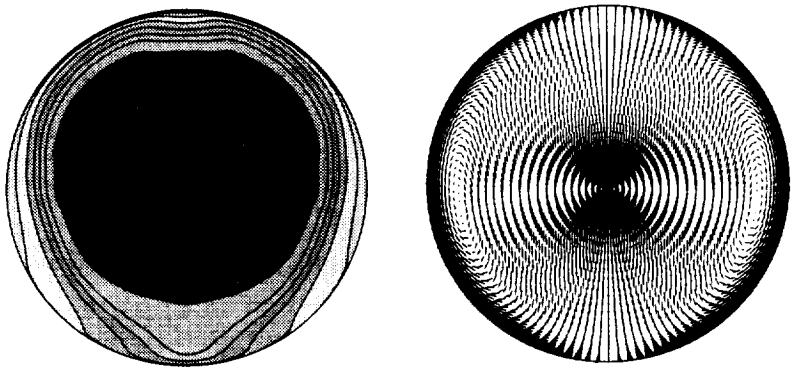

(a) Total PressureRecovery (b) Secondary Flow Velocity

Figure (23): Optimal Robust Maximum Performance installation engine face CFD solutions, $\Delta X/c = 2.0$, Re = 20.0 x 10^6/ft., $\alpha = 20.0^o$.

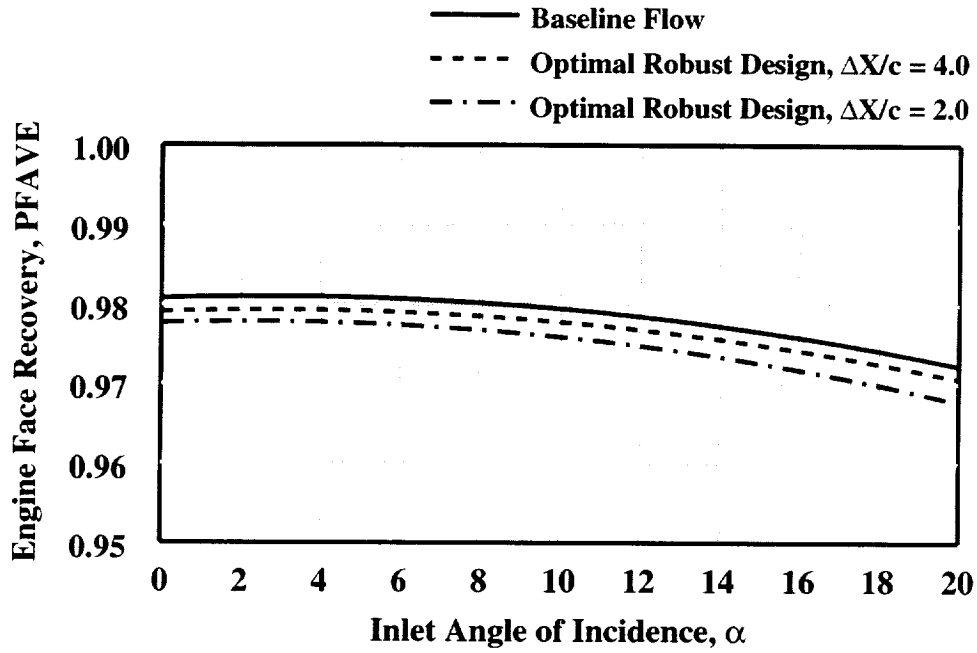

(a) Total Pressure Recovery Characteristics

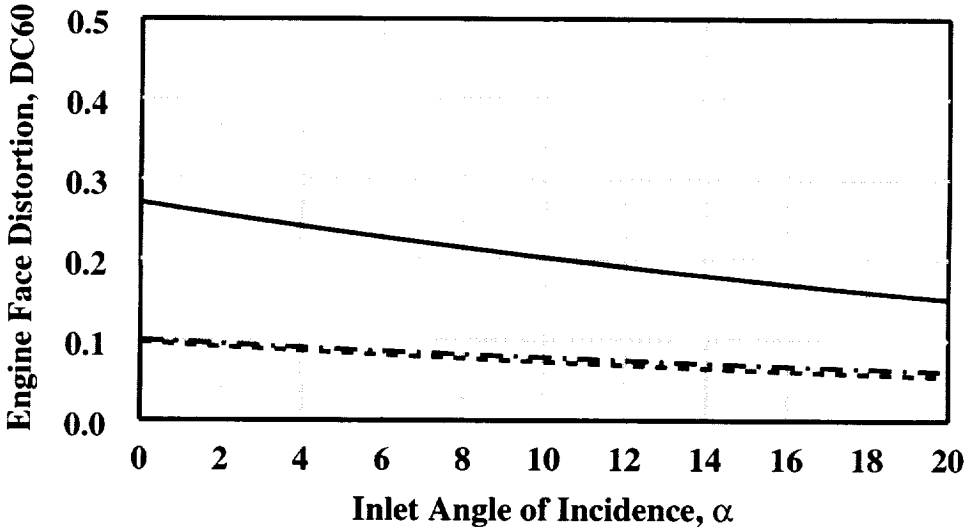

(b) Engine Face DC60 Distortion Characteristics

Figure (24): Effect of installation band spacing (ΔX/c) on inlet performance for Optimal Robust Maximum Performance installation design, Re = 20.0 x 10^6/ft.

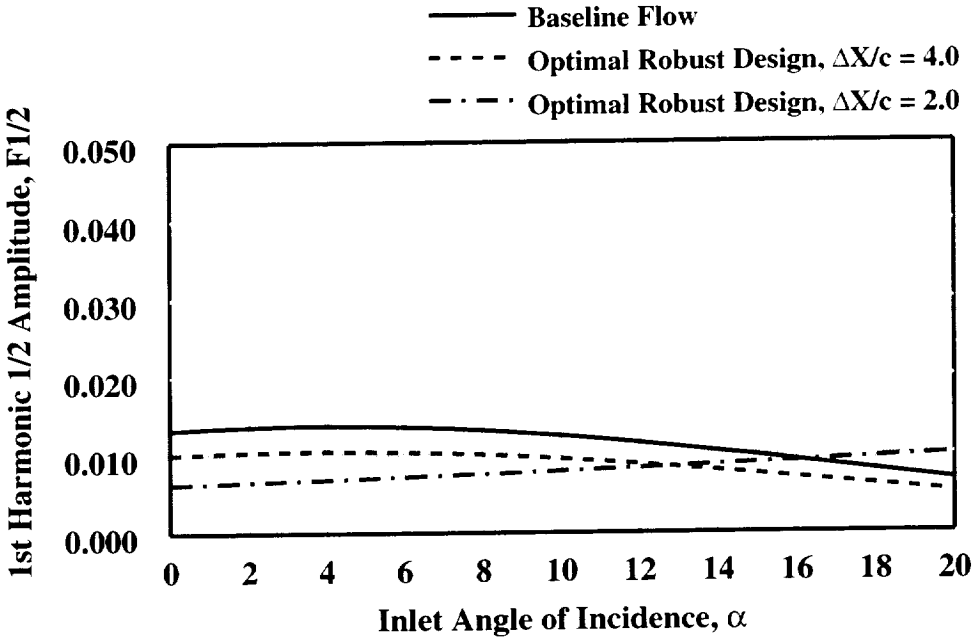

(c) 1st Fourier Harmonic 1/2 Amplitude Characteristics

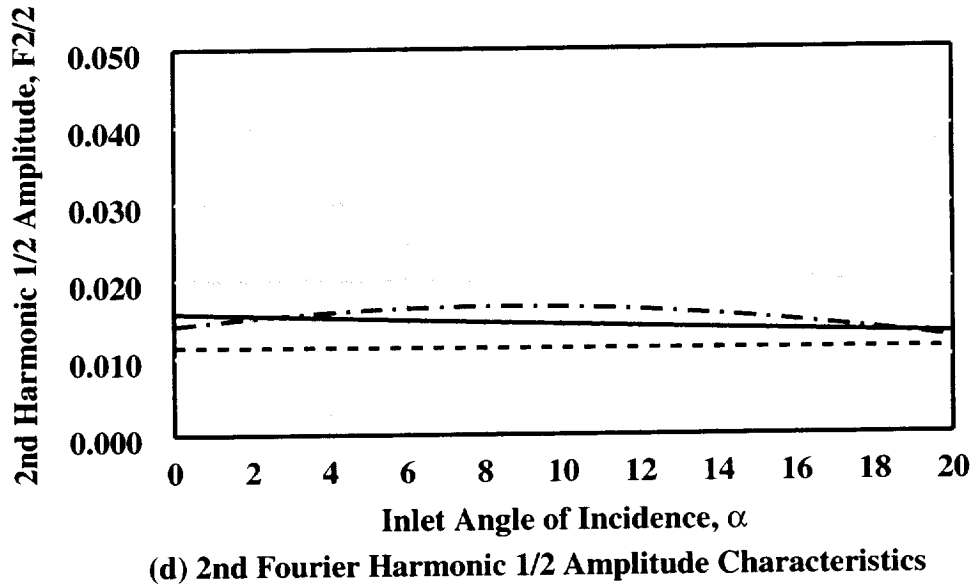

(d) 2nd Fourier Harmonic 1/2 Amplitude Characteristics

Figure (24): Effect of installation band spacing (ΔX/c) on inlet performance for Optimal Robust Maximum Performance installation design, Re = 20.0 x 10^6/ft.

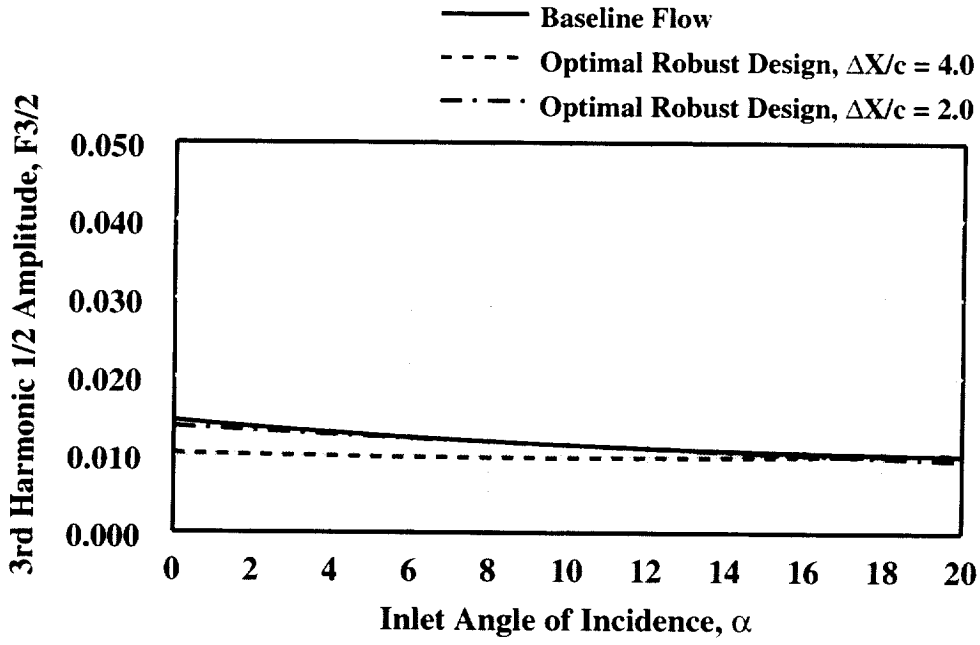

(e) 3rd Fourier Harmonic 1/2 Amplitude Characteristics

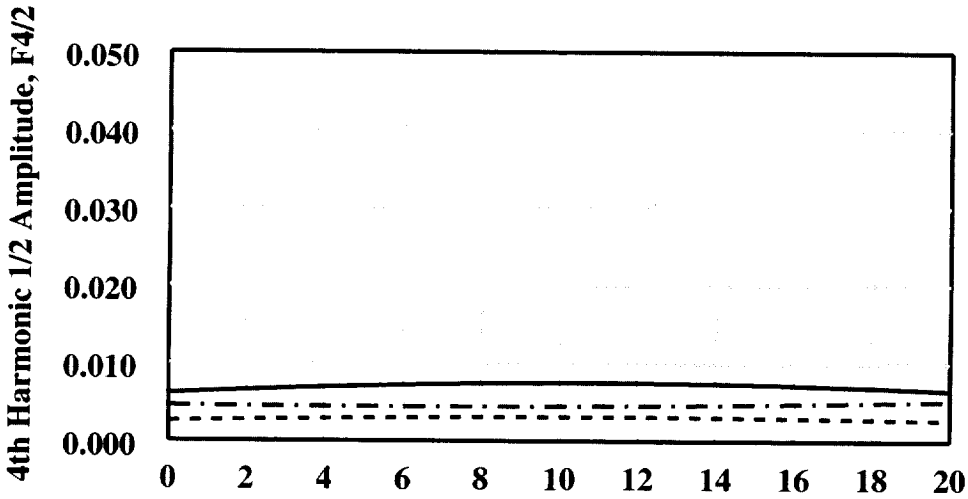

(f) 4th Fourier Harmonic 1/2 Amplitude Characteristics

Figure (24): Effect of installation band spacing (ΔX/c) on inlet performance for Optimal Robust Maximum Performance installation design, Re = 20.0 x 10^6/ft.

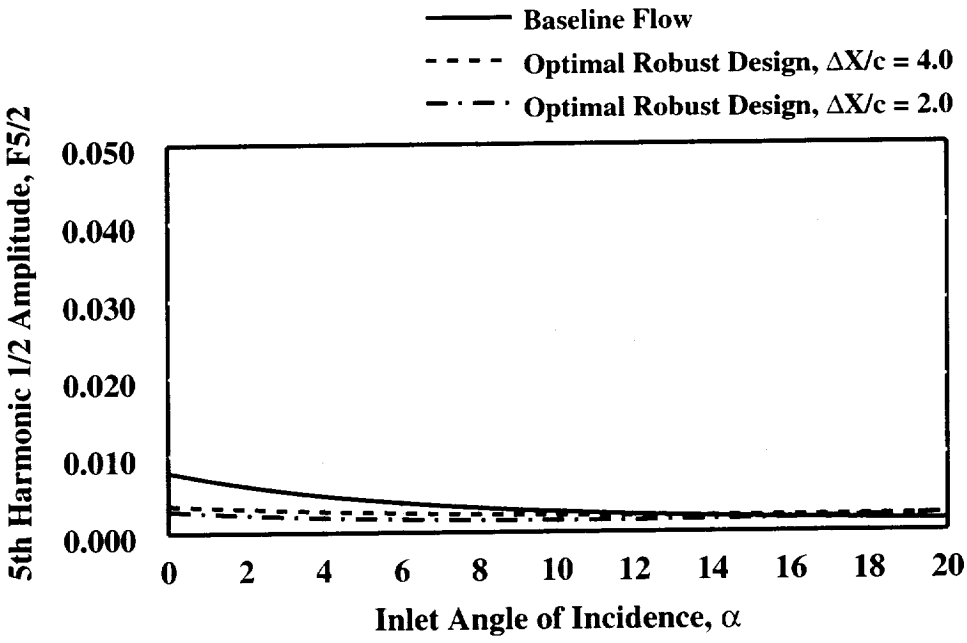

(g) 5th Fourier Harmonic 1/2 Amplitude Characteristics

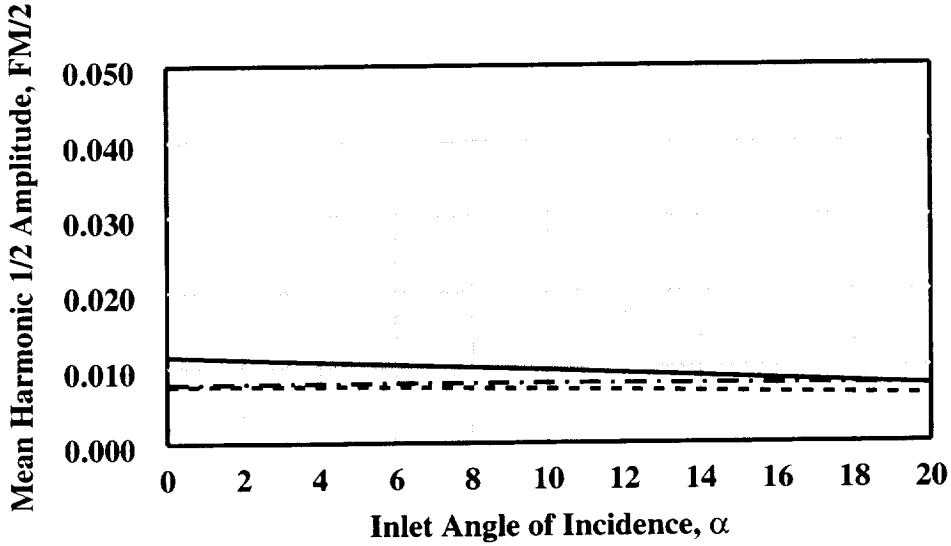

(h) Mean Fourier Harmonic 1/2 Amplitude Characteristics

Figure (24): Effect of installation band spacing (ΔX/c) on inlet performance for Optimal Robust Maximum Performance installation design, Re = 20.0 x 10^6/ft.

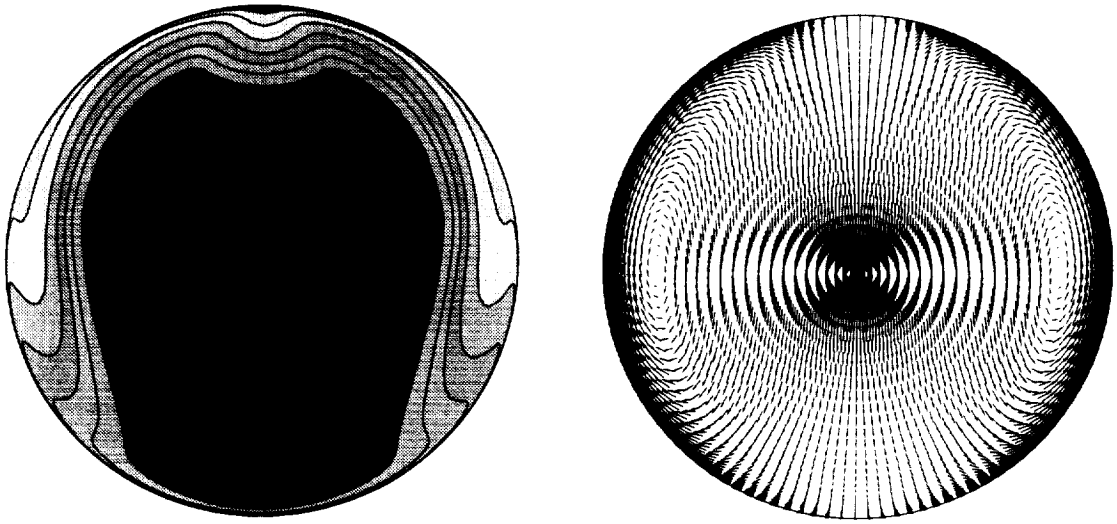

(a) Total Pressure Recovery (b) Secondary Flow Velocity

Figure (25): Optimal Robust Maximum HCF Life Expectancy installation engine face CFD solution, $\Delta X/c = 4.0$, $Re = 20.0 \times 10^6$/ft., $\alpha = 0.0^o$.

Factor/Response	Range/Constraint	Optimal Value
h_1	0.0 to 2.0	0.2
h_2	0.0 to 2.0	1.0
h_3	0.0 to 2.0	2.0
PFAVE	Unconstrained	0.97718
DC60	≤ 0.10	0.08399
F1/2	Minimized	0.01231
F2/2	Minimized	0.01487
F3/2	Minimized	0.00655
F4/2	Minimized	0.00748
F5/2	Minimized	0.00166

Table (12): Optimal Robust Maximum HCF Life Expectancy installation inlet CFD performance, $\Delta X/c = 4.0$, $Re = 20.0 \times 10^6$/ft., $\alpha = 0.0^o$.

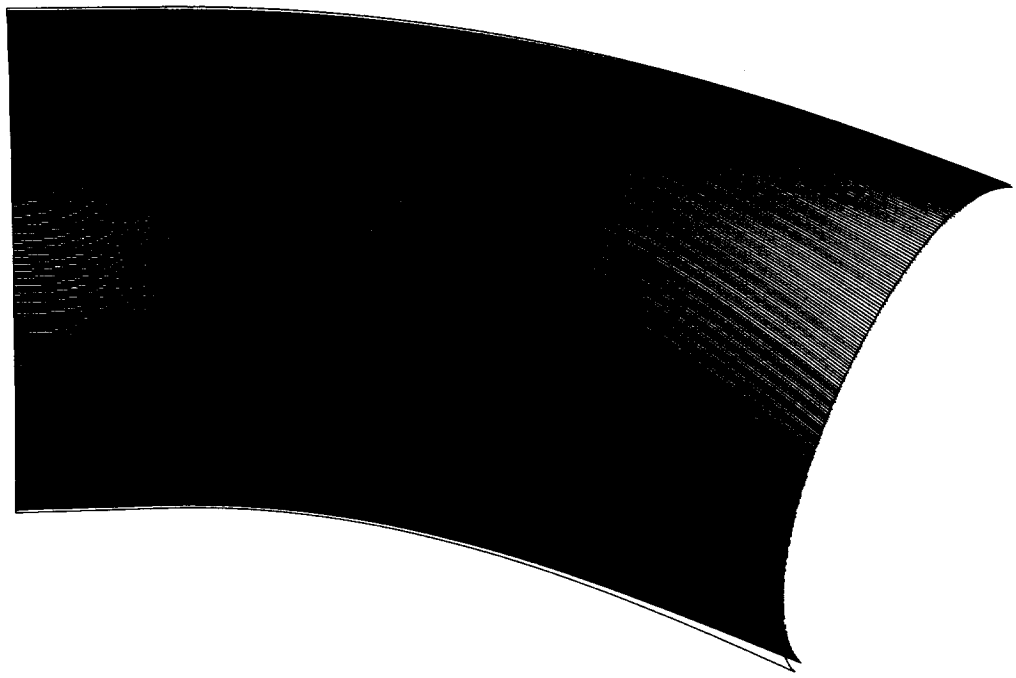

Figure(26): Near wall streamlines within effector region, baseline CFD solution, Re = 20.0 x 10^6/ft., $\alpha = 0.0^o$.

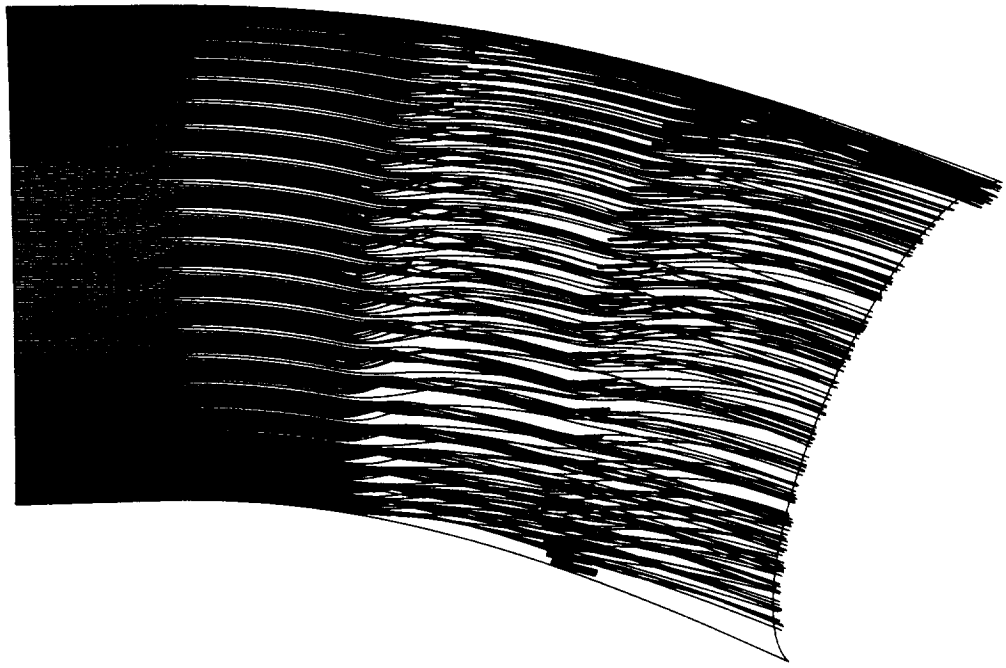

Figure (27): Near wall streamlines, Optimal Robust Maximum HCF Life Expectancy CFD solution, $\Delta X/c = 4.0$, Re = 20.0 x 10^6/ft., $\alpha = 0.0^o$.

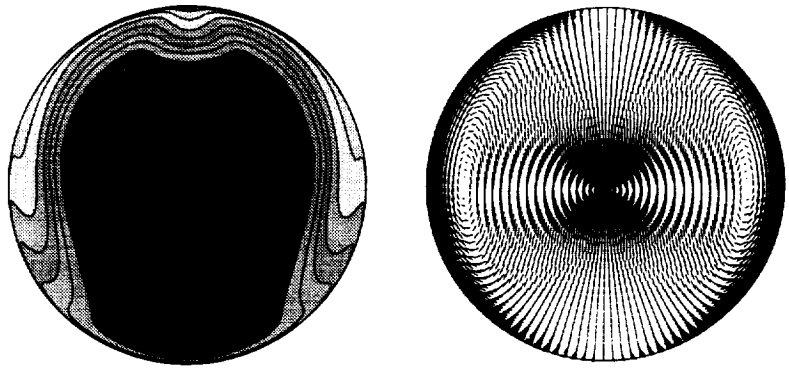

(a) Total Pressure Recovery (b) Secondary Flow Velocity

Figure (28): Optimal Robust Maximum HCF Life Expectancy installation engine face CFD solution, $\Delta X/c = 4.0$, Re = 20.0 x 10^6/ft., $\alpha = 0.0^o$.

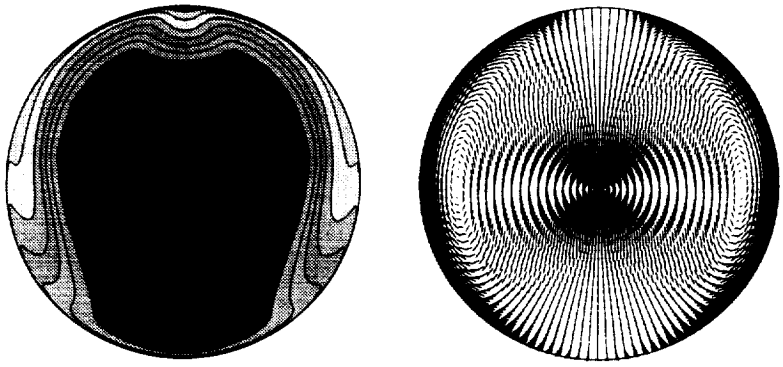

(a) Total Pressure Recovery (b) Secondary Flow Velocity

Figure (29): Optimal Robust Maximum HCF Life Expectancy installation engine face CFD solution, $\Delta X/c = 4.0$, Re = 20.0 x 10^6/ft., $\alpha = 10.0^o$.

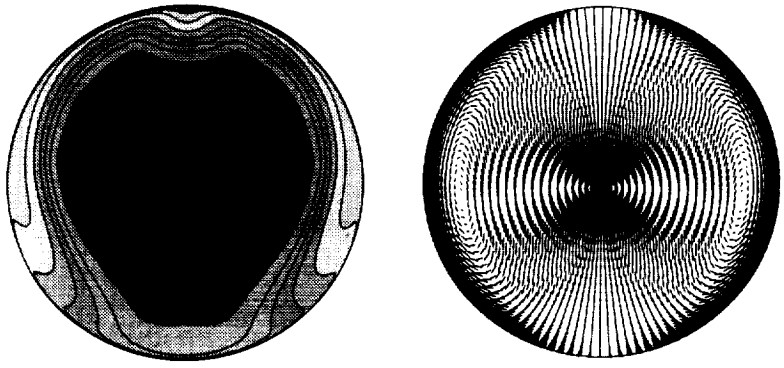

(a) Total Pressure Recovery (b) Secondary Flow Velocity

Figure (30): Optimal Robust Maximum HCF Life Expectancy installation engine face CFD solution, $\Delta X/c = 4.0$, Re = 20.0 x 10^6/ft., $\alpha = 20.0^o$.

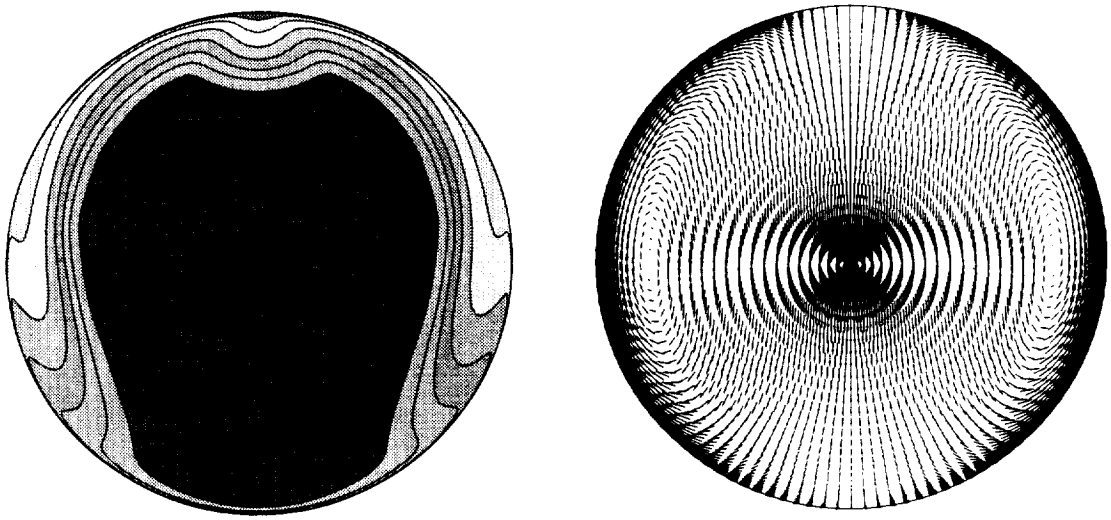

(a) Total pressure recovery (b) Secondary flow velocity

Figure (31): Optimal Maximum HCF Life Expectancy installation engine face CFD solution, $\Delta X/c = 2.0$, Re = 20.0 x 10^6/ft., $\alpha = 0.0^o$.

Factor/Response	Range/Constraint	Optimal Value
h_1	0.0 to 2.0	0.5
h_2	0.0 to 2.0	0.2
h_3	0.0 to 2.0	2.0
PFAVE	Unconstrained	0.97652
DC60	≤ 0.10	0.07950
F1/2	Minimized	0.01234
F2/2	Minimized	0.01488
F3/2	Minimized	0.00644
F4/2	Minimized	0.00343
F5/2	Minimized	0.00122

Table (13): Optimal Robust Maximum HCF Life Expectancy installation inlet CFD performance, $\Delta X/c = 2.0$, Re = 20.0 x 10^6/ft., $\alpha = 0.0^o$.

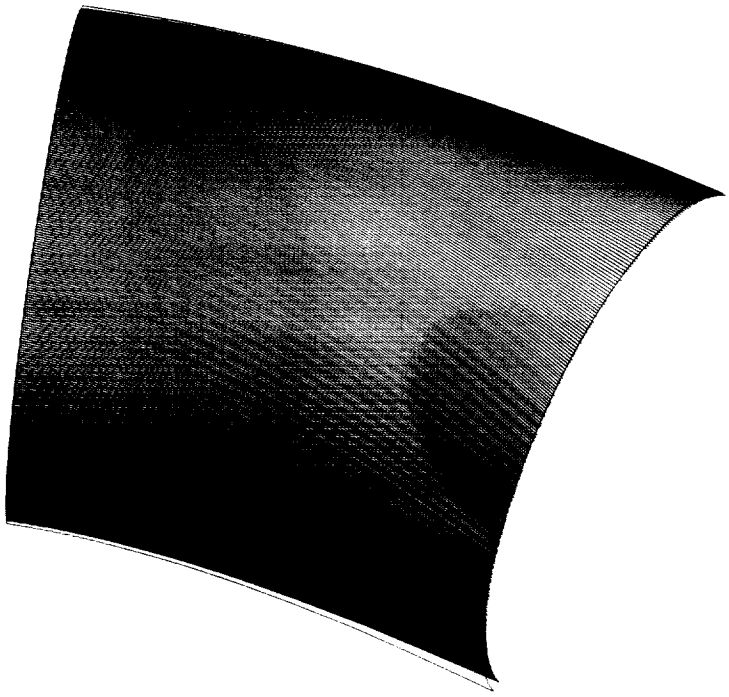

Figure(32): Near wall streamlines within effector region, baseline CFD solution, Re = 20.0 x 10^6/ft., α = 0.0.

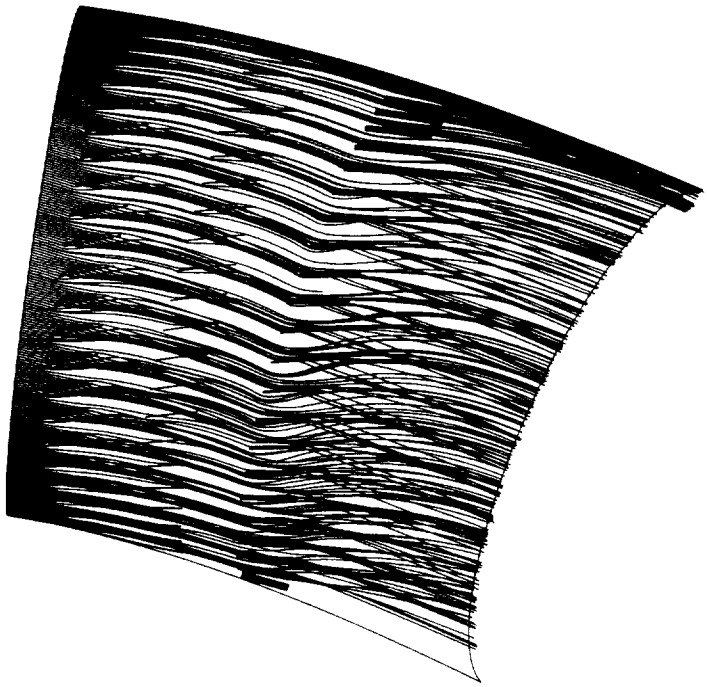

Figure (33): Near wall streamlines, Optimal Robust Maximum HCF Life Expectancy CFD solution, Re = 20.0 x 10^6/ft., $\alpha = 0.0^o$.

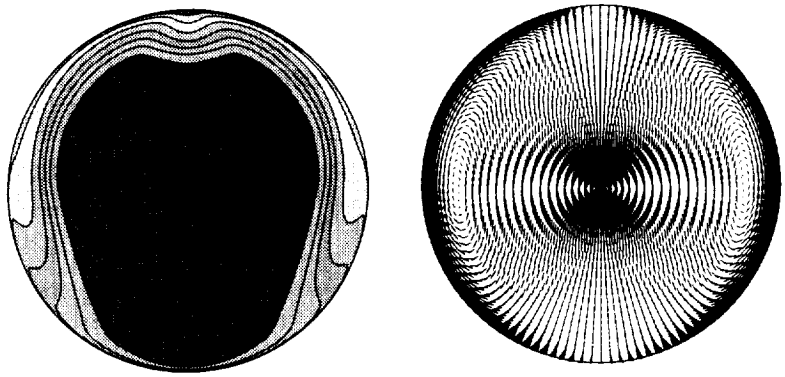

(a) Total Pressure Recovery (b) Secondary Flow Velocity

Figure (34): Optimal Robust Maximum HCF Life Expectancy installation engine face CFD solution, $\Delta X/c = 2.0$, Re = 20.0 x 10^6/ft., $\alpha = 0.0^o$.

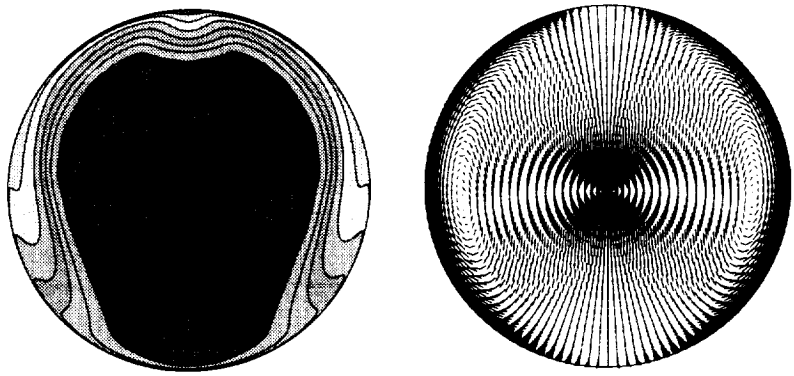

(a) Total Pressure Recovery (b) Secondary Flow Velocity

Figure (35): Optimal Robust Maximum HCF Life Expectancy installation engine face CFD solution, $\Delta X/c = 2.0$, Re = 20.0 x 10^6/ft., $\alpha = 10.0^o$.

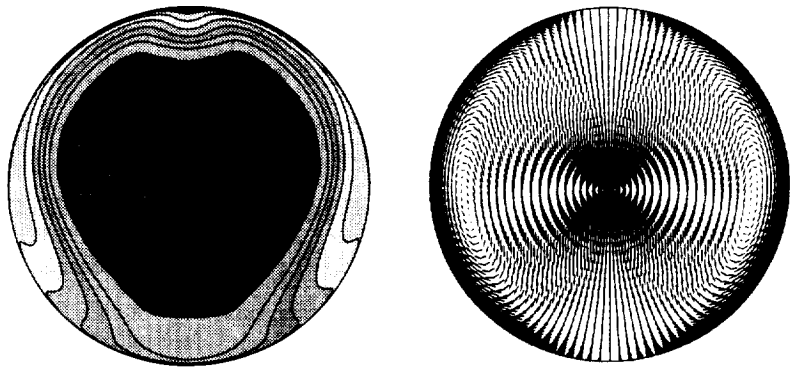

(a) Total Pressure Recovery (b) Secondary Flow Velocity

Figure (36): Optimal Robust Maximum HCF Life Expectancy installation engine face CFD solution, $\Delta X/c = 2.0$, Re = 20.0 x 10^6/ft., $\alpha = 20.0^o$.

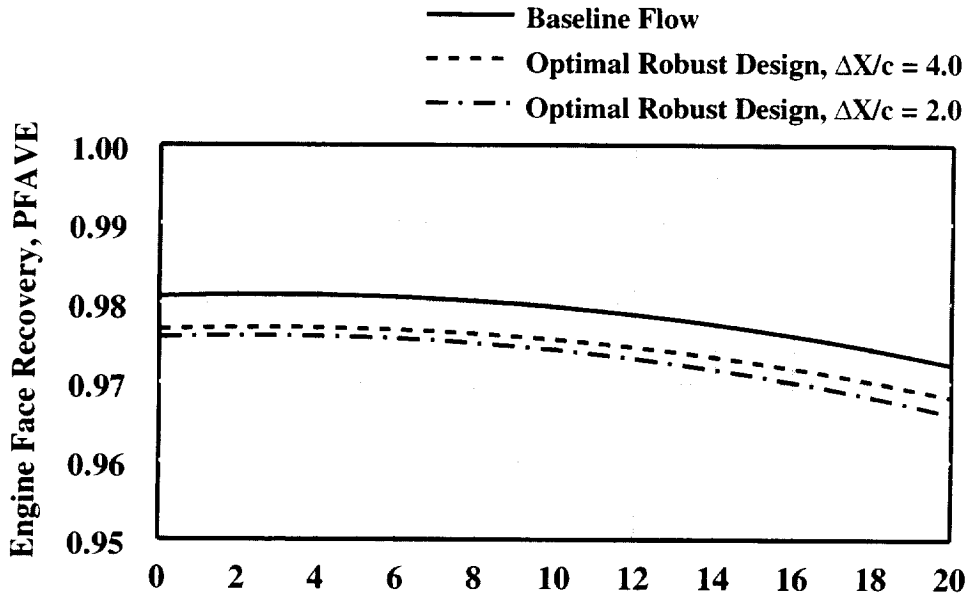

(a) Total Pressure Recovery Characteristics

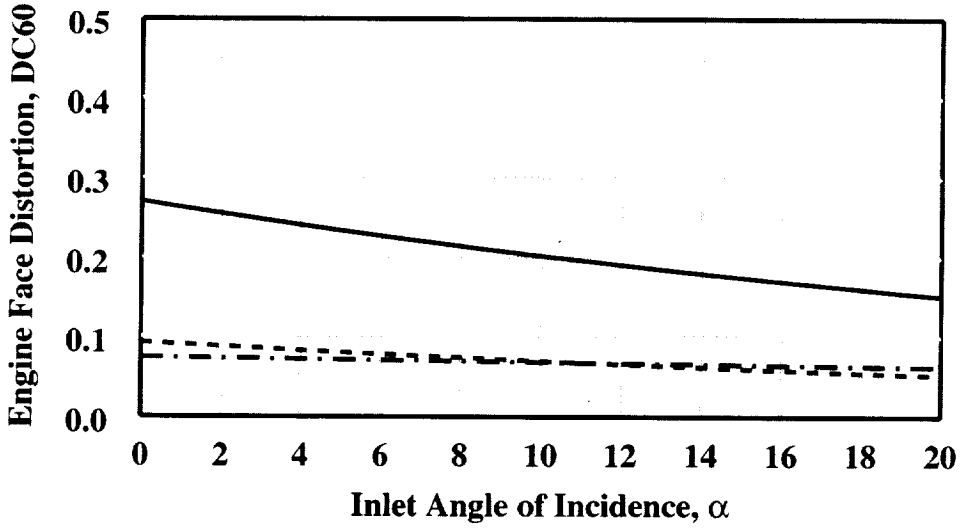

(b) Engine Face DC60 Distortion Characteristics

Figure (37): Effect of installation band spacing (ΔX/c) on inlet performance for Optimal Robust Maximum HCF Life Expectancy installation design, Re = 20.0 x 10^6/ft.

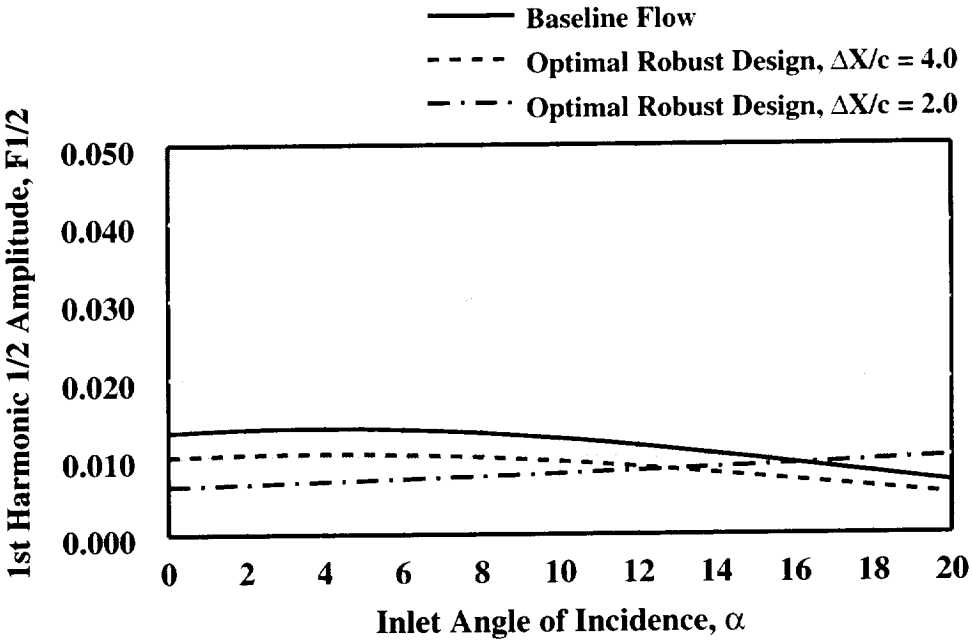

(c) 1st Fourier Harmonic 1/2 Amplitude Characteristics

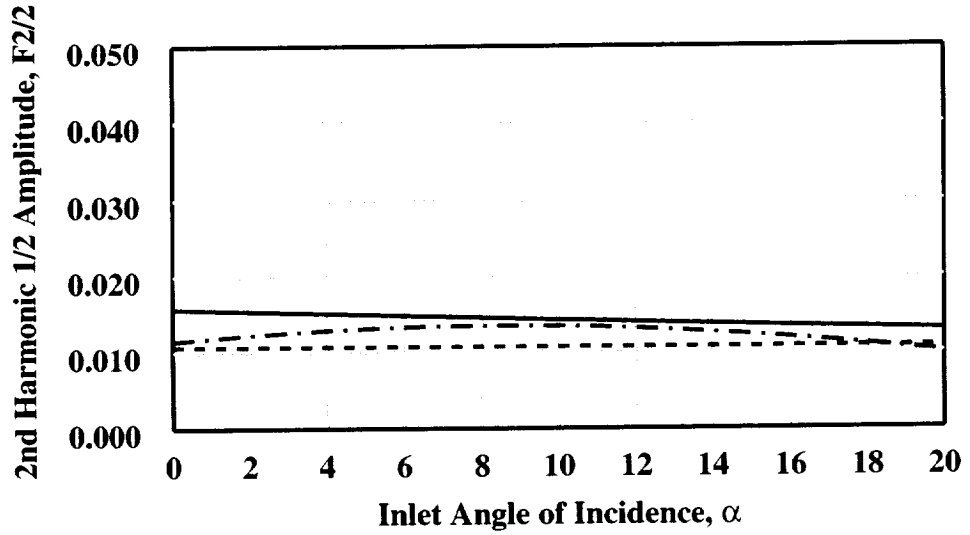

(d) 2nd Fourier Harmonic 1/2 Amplitude Characteristics

Figure (37): Effect of installation band spacing (ΔX/c) on inlet performance for Optimal Robust Maximum HCF Life Expectancy installation design, Re = 20.0 x 10^6/ft.

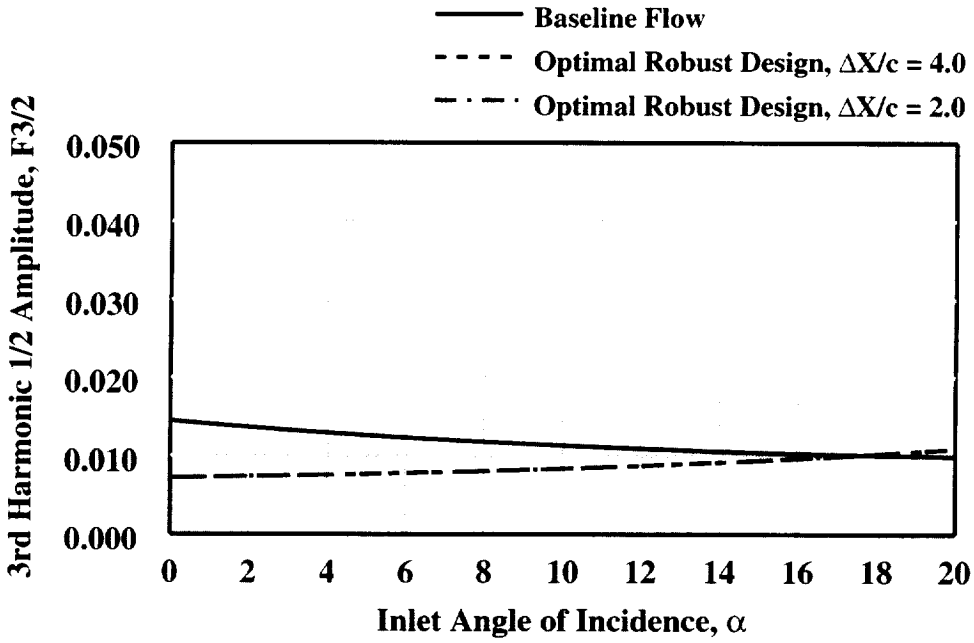

(e) 3rd Fourier Harmonic 1/2 Amplitude Characteristics

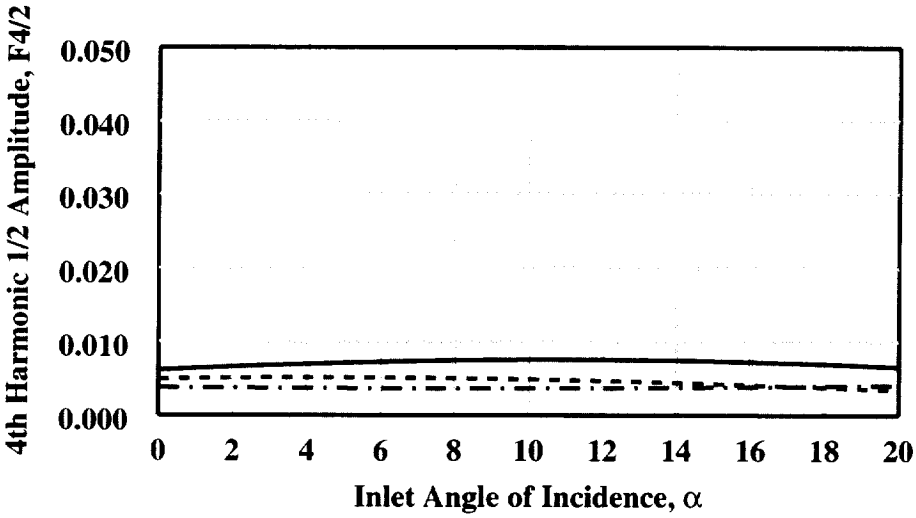

(f) 4th Fourier Harmonic 1/2 Amplitude Characteristics

Figure (37): Effect of installation band spacing (ΔX/c) on inlet performance for Optimal Robust Maximum HCF Life Expectancy installation design, Re = 20.0 x 10^6/ft.

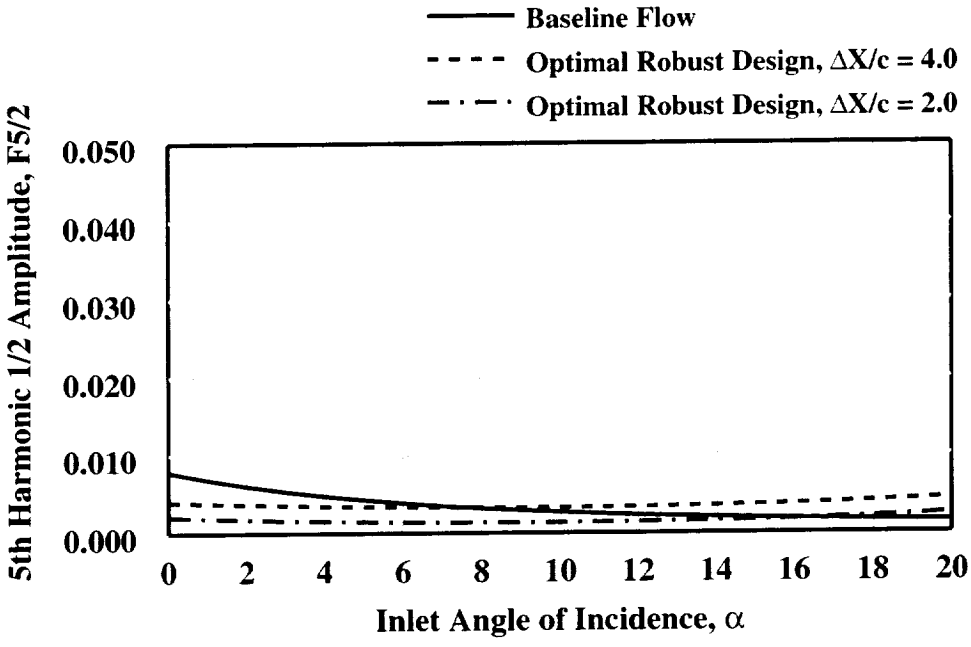

(g) 5th Fourier Harmonic 1/2 Amplitude Characteristics

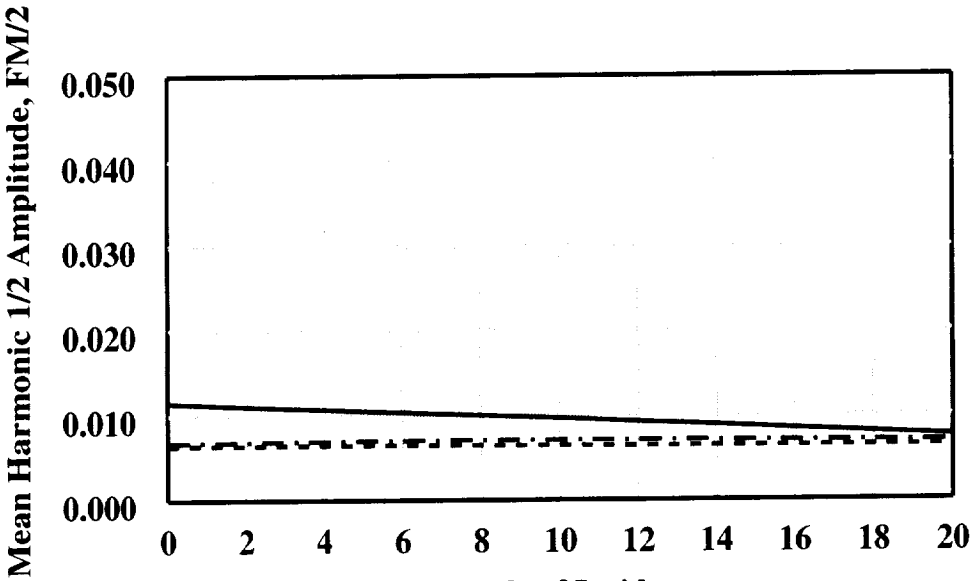

(h) Mean Fourier Harmonic 1/2 Amplitude Characteristics

Figure (37): Effect of installation band spacing (ΔX/c) on inlet performance for Optimal Robust Maximum HCF Life Expectancy installation design, Re = 20.0 x 10^6/ft.

Config.	DOE	ΔX/c	Re/ft.	h_1	h_2	h_3	α
nvg728	No. 7	4.0	$4.0x10^6$	0.0	0.0	2.00	0.0
nvg729			$12.0x10^6$	0.0	0.0	1.60	0.0
nvg730			$20.0x10^6$	0.0	0.0	1.90	0.0
nvg731			$20.0x10^6$	0.0	0.0	1.90	10.0
nvg732			$20.0x10^6$	0.0	0.0	1.90	20.0
nvg828	No. 8	2.0	$4.0x10^6$	0.0	0.0	1.90	0.0
nvg829			$12.0x10^6$	0.0	0.10	1.50	0.0
nvg830			$20.0x10^6$	0.0	0.10	1.50	0.0
nvg831			$20.0x10^6$	0.0	0.10	1.50	10.0
nvg832			$20.0x10^6$	0.0	0.10	1.50	20.0

Table (14): Optimal Robust Maximum Performance mission confirmation CFD analysis installations.

Config.	PFAVE	DC60	F1/2	F2/2	F3/2	F4/2	F5/2
nvg728	0.97377	0.08216	0.00788	0.01817	0.01683	0.00534	0.00152
nvg729	0.97872	0.06828	0.00894	0.01838	0.01387	0.00640	0.00080
nvg730	0.98021	0.06929	0.01472	0.01439	0.00860	0.00561	0.00148
nvg731	0.97888	0.06634	0.01344	0.01425	0.00785	0.00613	0.00130
nvg732	0.97064	0.05178	0.00752	0.01271	0.01360	0.00328	0.00220
nvg828	0.97202	0.08337	0.01150	0.01812	0.01229	0.00371	0.00199
nvg829	0.97639	0.06810	0.00812	0.01361	0.01748	0.00307	0.00119
nvg830	0.97794	0.06756	0.00903	0.01512	0.00906	0.00499	0.00177
nvg831	0.97670	0.06326	0.00970	0.01570	0.00989	0.00499	0.00115
nvg832	0.96903	0.05390	0.00650	0.00943	0.01126	0.00387	0.00260

Table (15): Optimal Robust Maximum Performance mission confirmation CFD analysis results.

Config.	DOE	ΔX/c	Re/ft.	h_1	h_2	h_3	α
nvg733	No. 7	4.0	$4.0x10^6$	0.10	0.10	2.0	0.0
nvg734			$12.0x10^6$	0.0	1.20	2.0	0.0
nvg735			$20.0x10^6$	0.20	1.10	2.0	0.0
nvg736			$20.0x10^6$	0.20	1.10	2.0	10.0
nvg737			$20.0x10^6$	0.20	1.10	2.0	20.0
nvg833	No. 8	2.0	$4.0x10^6$	0.0	1.30	2.0	0.0
nvg834			$12.0x10^6$	0.10	0.80	2.0	0.0
nvg835			$20.0x10^6$	0.50	0.20	2.0	0.0
nvg836			$20.0x10^6$	0.50	0.20	2.0	10.0
nvg837			$20.0x10^6$	0.50	0.20	2.0	20.0

Table (16): Optimal Robust Maximum HCF Life Expectancy mission confirmation CFD analysis installations.

Config.	PFAVE	DC60	F1/2	F2/2	F3/2	F4/2	F5/2
nvg733	0.97301	0.09267	0.00807	0.01822	0.01696	0.00175	0.00072
nvg734	0.97521	0.08757	0.01200	0.01845	0.00864	0.00713	0.00157
nvg735	0.97718	0.08399	0.01231	0.01487	0.00655	0.00748	0.00166
nvg736	0.97595	0.08125	0.01228	0.01294	0.00766	0.00710	0.00161
nvg737	0.96799	0.06926	0.00780	0.01265	0.01002	0.00242	0.00139
nvg833	0.97018	0.09509	0.01200	0.01582	0.00978	0.00582	0.00108
nvg834	0.97472	0.08213	0.01278	0.01264	0.01106	0.00513	0.00097
nvg835	0.97652	0.07950	0.01234	0.01488	0.00644	0.00343	0.00122
nvg836	0.97528	0.07746	0.01102	0.01482	0.00878	0.00482	0.00108
nvg837	0.96761	0.06058	0.00516	0.01130	0.01083	0.00318	0.00194

Table (17): Optimal Robust Maximum HCF Life Expectancy mission confirmation CFD analysis results.

Factor	α	LOG(Y_{DOE})	LOG(Y_{CFD})	t	t*	Comment
PFAVE	0.0°	0.979086	0.980210	2.079614	1.871486	Not Diff.
DC60		-2.333777	-2.669455	2.109816	1.814753	Not Diff.
F1/2		-4.602175	-4.218548	1.968293	0.716501	Not Diff.
F2/2		-4.478538	-4.241222	1.968121	0.535710	Not Diff.
F3/2		-4.580673	-4.755993	1.968382	1.626633	Not Diff.
F4/2		-5.965407	-5.183205	1.968352	2.407535	Diff.
F5/2		-5.638557	-6.515713	1‘.968264	1.363719	Not Diff.
PFAVE	10.0°	0.977822	0.097880	2.079614	1.693789	Not Diff.
DC60		-2.625508	-2.712962	2.109816	0.409986	Not Diff.
F1/2		-4.664390	-4.309520	1.968293	0.654631	Not Diff.
F2/2		-4.491395	-4.250998	1.968121	0.546140	Not Diff.
F3/2		-4.645055	-4.847242	1.968382	1.948857	Not Diff.
F4/2		-5.762578	-5.272650	1.968352	1.511414	Not Diff.
F5/2		-6.129807	-6.645391	1.968264	0.801996	Not Diff.
PFAVE	20.0°	0.970562	0.970640	2.079614	0.129457	Not Diff.
DC60		-2.917235	-2.960751	2.109816	0.235152	Not Diff.
F1/2		-5.270313	-5.649294	1.968293	0.714093	Not Diff.
F2/2		-4.505149	-4.536577	1.968121	0.073335	Not Diff.
F3/2		-4.492649	4.456901	1.968382	0.452979	Not Diff.
F4/2		-5.896882	-6.083580	1.968352	0.578990	Not Diff.
F5/2		-6.112954	-6.725434	1.968264	0.959037	Not Diff.

Table (18): Comparison of DOE predicted and CFD analysis Optimal Robust Maximum Performance installations, $\Delta X/c = 4.0$, Re = 20.0 x 10^6/ft.

Factor	α	LOG(Y_{DOE})	LOG(Y_{CFD})	t	t*	Comment
PFAVE	0.0°	0.977710	0.977940	2.085963	0.235297	Not Diff.
DC60		-2.304056	-2.694739	2.059363	2.035742	Not Diff.
F1/2		-5.612754	-4.707203	1.968264	1.845633	Not Diff.
F2/2		-4.259809	-4.260163	1.968093	0.000634	Not Diff.
F3/2		-4.291747	-4.820842	1.968382	0.411848	Not Diff.
F4/2		-5.391749	-5.523964	1.968178	0.757755	Not Diff.
F5/2		-5.863247	-6.668738	1.968293	1.704033	Not Diff.
PFAVE	10.0°	0.975923	0.976700	2.085963	0.759509	Not Diff.
DC60		-2.550752	-2.760502	2.059363	1.140861	Not Diff.
F1/2		-5.158555	-4.744432	1.968264	0.860005	Not Diff.
F2/2		-4.103789	-4.290359	1.968093	0.331830	Not Diff.
F3/2		-4.484015	-4.616231	1.968382	1.367116	Not Diff.
F4/2		-5.398580	-5.523964	1.968178	0.733498	Not Diff.
F5/2		-6.504292	-6.785538	1.968293	0.608148	Not Diff.
PFAVE	20.0°	0.967658	0.969030	2.085963	1.389292	Not Diff.
DC60		-2.797439	-2.920625	2.059363	0.640338	Not Diff.
F1/2		-4.704549	-5.035953	1.968264	0.678226	Not Diff.
F2/2		-4.393775	-4.663859	1.968093	0.483541	Not Diff.
F3/2		-4.6775237	-4.579502	1.968382	0.892126	Not Diff.
F4/2		-5.252579	-5.554501	1.968178	1.760081	Not Diff.
F5/2		-6.084457	-5.952244	1.968293	0.281273	Not Diff.

Table (19): Comparison of DOE predicted and CFD analysis optimal Robust Maximum Performance installations, $\Delta X/c = 2.0$, Re = 20.0 x 10^6/ft.

Factor	α	LOG(Y_{DOE})	LOG(Y_{CFD})	t	t*	Comment
PFAVE	0.0°	0.976651	0.977180	2.079614	0.898054	Not Diff.
DC60		-2.375909	-2.477058	2.109816	0.582456	Not Diff.
F1/2		-5.268564	-4.179249	1.968293	1.950373	Not Diff.
F2/2		-4.442541	-4.082218	1.968121	0.810768	Not Diff.
F3/2		-4.929378	-5.028290	1.968382	0.934985	Not Diff.
F4/2		-5.310795	-4.895522	1.968352	1.301174	Not Diff.
F5/2		-5.523713	-6.400938	1'.968264	1.348780	Not Diff.
PFAVE	10.0°	0.975388	0.975950	2.079614	0.925371	Not Diff.
DC60		-2.667638	-2.510224	2.109816	0.945961	Not Diff.
F1/2		-5.330841	-4.428895	1.968293	1.973281	Diff.
F2/2		-4.440249	-4.078078	1.968121	0.818767	Not Diff.
F3/2		-4,781788	-4.871743	1.968382	0.854385	Not Diff.
F4/2		-5.323430	-4.947660	1.968352	1.188150	Not Diff.
F5/2		-5.730640	-6.431521	1.968264	1.073598	Not Diff.
PFAVE	20.0°	0.968127	0.967990	2.079614	0.232577	Not Diff.
DC60		-2.959381	-2.669888	2.109816	1.671469	Not Diff.
F1/2		-5.936598	-4.853632	1.968293	1.954692	Not Diff.
F2/2		-4.438047	-4.157284	1.968121	0.631394	Not Diff.
F3/2		-4.517526	-4.341269	1.968382	1.661406	Not Diff.
F4/2		-5.672865	-5.678115	1.968352	0.016354	Not Diff.
F5/2		-5.429338	-6.036462	1.968264	0.935661	Not Diff.

Table (20): Comparison of DOE predicted and CFD analysis Optimal Robust Maximum HCF Life Expectancy installations, $\Delta X/c = 4.0$, $Re = 20.0 \times 10^6$/ft.

Factor	α	LOG(Y_{DOE})	LOG(Y_{CFD})	t	t*	Comment
PFAVE	0.0°	0.975688	0.,975688	2.085963	0.860447	Not Diff.
DC60		-2.495054	-2.531998	2.059363	0.191579	Not Diff.
F1/2		-5.079021	-4.177291	1.968264	1.861285	Not Diff.
F2/2		-4.467410	-4.081626	1.968093	0.689597	Not Diff.
F3/2		-4.595220	-4.774773	1.968382	1.700002	Not Diff.
F4/2		-5.573281	-5.046781	1.968178	3.021162	Diff.
F5/2		-6.179113	-6.708904	1.968293	1.127054	Not Diff.
PFAVE	10.0°	0.974086	0.975280	2.085963	1.177051	Not Diff.
DC60		-2.741741	-2.557994	2.059363	0.994836	Not Diff.
F1/2		-4.844316	-4.268698	1.968264	1.196707	Not Diff.
F2/2		-4.311382	-4.085187	1.968093	0.404538	Not Diff.
F3/2		-4.701351	-4.627416	1.968382	0.808647	Not Diff.
F4/2		-5.611933	-5.334981	1.968178	1.635816	Not Diff.
F5/2		-6.621825	-6.830794	1.968293	0.480715	Not Diff.
PFAVE	20.0°	0.966004	0.967610	2.085963	1.661734	Not Diff.
DC60		-2.988439	-2.803790	2.059363	0.902363	Not Diff.
F1/2		-4.609479	-5.266819	1.968264	1.346944	Not Diff.
F2/2		-4.601377	-4.247496	1.968093	0.632085	Not Diff.
F3/2		-4.807531	-4.280915	1.968382	5.064411	Diff.
F4/2		-5.497744	-5.575087	1.968178	1.467392	Not Diff.
F5/2		-6.013301	-6.425067	1.968293	0.491379	Not Diff.

Table (21): Comparison of DOE predicted and CFD analysis Optimal Robust Maximum HCF Life Expectancy installations, $\Delta X/c = 2.0$, Re = 20.0 x 10^6/ft.

Factor	Re/ft	LOG($Y_{4.0}$)	LOG($Y_{2.0}$)	t	t*	Comment
PFAVE	$4.0x10^6$	0.974013	0.971753	2.082789	1.954998	Not Diff.
DC60		-2.539980	-2.496048	2.097889	0.162931	Not Diff.
F1/2		-4.535178	-5.316685	1.968279	1.055847	Not Diff.
F2/2		-4.184094	-4.047728	1.968107	0.190680	Not Diff.
F3/2		-4.160997	-4.425101	1.968382	1.997421	Diff.
F4/2		-6.360212	-5.357006	1.968265	2.529900	Diff.
F5/2		-6.642319	-6.592215	1.968279	0.062667	Not Diff.
PFAVE	$12.0x10^6$	0.978526	0.977008	2.082789	1.299935	Not Diff.
DC60		-2.352784	-2.313535	2.097889	0.157850	Not Diff.
F1/2		-4.353245	-5.710807	1.968279	1.862035	Not Diff.
F2/2		-4.271129	-4.333389	1.968107	0.087071	Not Diff.
F3/2		-4.251279	-4.350683	1.968382	0.719597	Not Diff.
F4/2		-6.082803	-5.453569	1.968265	1.706588	Not Diff.
F5/2		-4.174037	-6.637728	1.968279	0.281488	Not Diff.
PFAVE	$20.0x10^6$	0.979086	0.977710	2.082789	1.199386	Not Diff.
DC60		-2.333777	-2.304056	2.097889	0.111503	Not Diff.
F1/2		-4.602175	-5.612754	1.968279	1.391550	Not Diff.
F2/2		-4.478538	-4.259809	1.968107	0.306988	Not Diff.
F3/2		-4.580673	-4.291747	1.968382	1.833993	Not Diff.
F4/2		-5.965407	-5.391749	1.968265	1.555533	Not Diff.
F5/2		-5.638557	-5.863247	1.968279	0.281488	Not Diff.

Table (22): Comparison of band spacing DOE regression models for the Optimal Robust Maximum Performance installations, $\alpha = 0.0^o$.

Factor	α	LOG($Y_{4.0}$)	LOG($Y_{2.0}$)	t	t*	Comment
PFAVE	0.0°	0.979086	0.977710	2.082789	1.199386	Not Diff.
DC60		-2.333377	-2.304056	2.097889	0.111503	Not Diff.
F1/2		-4.602175	-5.612754	1.968279	1.391550	Not Diff.
F2/2		-4.478538	-4.259809	1.968107	0.306988	Not Diff.
F3/2		-4.580673	-4.291747	1.968382	1.833993	Not Diff.
F4/2		-5.965047	-5.391749	1.968265	1.555533	Not Diff.
F5/2		-5.638557	-5.863247	1.968279	0.281488	Not Diff.
PFAVE	10.0°	0.977822	0.975923	2.082789	1.584285	Not Diff.
DC60		-2.625508	-2.550752	2.097889	0.099241	Not Diff.
F1/2		-4.664390	-5.15855	1.968279	0.681534	Not Diff.
F2/2		-4.491395	-4.103789	1.968107	0.542823	Not Diff.
F3/2		-4.645055	-4.484015	1.968382	1.135425	Not Diff.
F4/2		-5.762578	-5.398580	1.968265	0.993273	Not Diff.
F5/2		-6.129807	-6.504292	1.968279	0.472874	Not Diff.
PFAVE	20.0°	0.970562	0.967658	2.082789	2.510279	Diff.
DC60		-2.917235	-2.794439	2.097889	0.4448786	Not Diff.
F1/2		-5.270313	-4.704549	1.968279	0.784254	Not Diff.
F2/2		-4.504149	-4.393775	1.968107	0.154932	Not Diff.
F3/2		-4.592649	-4.676237	1.968382	0.564102	Not Diff.
F4/2		-5.896882	-5.252579	1.968265	1.764040	Not Diff.
F5/2		-6.112954	-6.084457	1.968279	0.035937	Not Diff.

Table (23): Comparison of band spacing DOE regression models for the Optimal Robust Maximum Performance installations, Re = 20.0 x 10^6/ft.

Factor	Re/ft	LOG($Y_{4.0}$)	LOG($Y_{2.0}$)	t	t*	Comment
PFAVE	$4.0x10^6$	0.973677	0.969971	2.082789	3.213556	Diff.
DC60		-2.547259	-2.596097	2.097889	0.186664	Not Diff.
F1/2		-4.814288	-5.223952	1.968279	0.558576	Not Diff.
F2/2		-4.194585	-4.297244	1.968107	0.142537	Not Diff.
F3/2		-4.135854	-4.431973	1.968382	1.995098	Diff.
F4/2		-6.268536	-5.259481	1.868265	2.586249	Diff.
F5/2		-6.603954	-6.477272	1.968279	0.161384	Not Diff.
PFAVE	$12.0x10^6$	0.975941	0.975011	2.082789	0.780591	Not Diff.
DC60		-2.627485	-2.550188	2.097889	0.314034	Not Diff.
F1/2		-4.793792	-5.297318	1.968279	0.678542	Not Diff.
F2/2		-4.257122	-4.434500	1.968107	0.247539	Not Diff.
F3/2		-4.667791	4.576194	1.968382	0.640659	Not Diff.
F4/2		-5.627377	-5.481211	1.868265	0.127383	Not Diff.
F5/2		-6.306723	-6.714659	1.968279	0.520541	Not Diff.
PFAVE	$20.0x10^6$	0.976651	0.975688	2.082789	0.850531	Not Diff.
DC60		-2.375909	-2.495054	2.097889	0.459117	Not Diff.
F1/2		-5.268564	-5.079021	1.968279	0.256362	Not Diff.
F2/2		-4.442541	-4.467410	1.968107	0.034807	Not Diff.
F3/2		-4.929378	-4.595220	1.968382	2.235333	Diff.
F4/2		-5.310795	-5.573281	1.868265	0.721844	Not Diff.
F5/2		-5.523713	-6.170113	1.968279	0.800816	Not Diff.

Table (24): Comparison of band spacing DOE regression models for the Optimal Robust Maximum Performance installations, α =0.0°.

Factor	α	LOG($Y_{4.0}$)	LOG($Y_{2.0}$)	t	t*	Comment
PFAVE	0.0°	0.976651	0.975688	2.082789	0.850531	Not Diff.
DC60		-2.375909	-2.495054	2.097889	0.459117	Not Diff.
F1/2		-5.268564	-5.079021	1.968279	0.256362	Not Diff.
F2/2		-4.442541	-4.467410	1.968107	0.034807	Not Diff.
F3/2		-4.929378	-4.595220	1.968382	2.235333	Diff.
F4/2		-5.310795	-5.573281	1.868265	0.721844	Not Diff.
F5/2		-5.523713	-6.170113	1.968279	0.800816	Not Diff.
PFAVE	10.0°	0.975388	0.974086	2.082789	1.101237	Not Diff.
DC60		-2.667638	-2.741741	2.097889	0.298075	Not Diff.
F1/2		-5.330841	-4.844316	1.968279	0.667040	Not Diff.
F2/2		-4.440249	-4.311382	1.968107	0.180751	Not Diff.
F3/2		-4.781788	-4.701351	1.968382	0.576841	Not Diff.
F4/2		-5.323430	-5.611933	1.868265	0.804234	Not Diff.
F5/2		-5.730640	-6.621825	1.968279	1.136249	Not Diff.
PFAVE	20.0°	0.968127	0.966004	2.082789	1.875732	Not Diff.
DC60		-2.959381	-2.988439	2.097889	0.108390	Not Diff.
F1/2		-5.936598	-4.609479	1.968279	1.794777	Not Diff.
F2/2		-4.438047	-4.601377	1.968107	0.228444	Not Diff.
F3/2		-4.517526	-4.807531	1.968382	1.952224	Not Diff.
F4/2		-5.672865	-5.497744	1.868265	0.480565	Not Diff.
F5/2		-5.429338	-6.013301	1.968279	0.727965	Not Diff.

Table (25): Comparison of band spacing DOE regression models for the Optimal Robust Maximum Performance installations, Re = 20.0 x 10^6/ft.

REPORT DOCUMENTATION PAGE

Form Approved
OMB No. 0704-0188

1. AGENCY USE ONLY (*Leave blank*)	2. REPORT DATE	3. REPORT TYPE AND DATES COVERED
	July 2002	Technical Memorandum

4. TITLE AND SUBTITLE

Optimal Micro-Scale Secondary Flow Control for the Management of High Cycle Fatigue and Distortion in Compact Inlet Diffusers

5. FUNDING NUMBERS

WU–708–53–13–00

6. AUTHOR(S)

Bernhard H. Anderson and Dennis J. Keller

7. PERFORMING ORGANIZATION NAME(S) AND ADDRESS(ES)

National Aeronautics and Space Administration
John H. Glenn Research Center at Lewis Field
Cleveland, Ohio 44135–3191

8. PERFORMING ORGANIZATION REPORT NUMBER

E–13415

9. SPONSORING/MONITORING AGENCY NAME(S) AND ADDRESS(ES)

National Aeronautics and Space Administration
Washington, DC 20546–0001

10. SPONSORING/MONITORING AGENCY REPORT NUMBER

NASA TM—2002-211686

11. SUPPLEMENTARY NOTES

Bernhard H. Anderson, NASA Glenn Research Center, and Dennis J. Keller, RealWorld Quality Systems, Cleveland, Ohio 44116. Responsible person, Bernhard H. Anderson, organization code 5850, 216–433–5822.

12a. DISTRIBUTION/AVAILABILITY STATEMENT

Unclassified - Unlimited
Subject Category: 07 Distribution: Nonstandard

Available electronically at http://gltrs.grc.nasa.gov/GLTRS

This publication is available from the NASA Center for AeroSpace Information, 301–621–0390.

12b. DISTRIBUTION CODE

13. ABSTRACT ***(Maximum 200 words)***

The purpose of this study on micro-scale secondary flow control (MSFC) is to study the aerodynamic behavior of micro-vane effectors through their factor (i.e., the design variable) interactions and to demonstrate how these statistical interactions, when brought together in an optimal manner, determine design robustness. The term micro-scale indicates the vane effectors are small in comparison to the local boundary layer height. Robustness in this situation means that it is possible to design fixed MSFC robust installation (i.e., open loop) which operates well over the range of mission variables and is only marginally different from adaptive (i.e., closed loop) installation design, which would require a control system. The inherent robustness of MSFC micro-vane effector installation designs comes about because of their natural aerodynamic characteristics and the manner in which these characteristics are brought together in an optimal manner through a structured Response Surface Methodology design process.

14. SUBJECT TERMS

Aeronautics; Propulsion; Fluid dynamics

15. NUMBER OF PAGES

69

16. PRICE CODE

17. SECURITY CLASSIFICATION OF REPORT	18. SECURITY CLASSIFICATION OF THIS PAGE	19. SECURITY CLASSIFICATION OF ABSTRACT	20. LIMITATION OF ABSTRACT
Unclassified	Unclassified	Unclassified	